

NATURAL GAS LIQUEFIER FOR VEHICLE FUEL

INTERIM REPORT
TFLRF No. 310

By

E.C. Owens
Southwest Research Institute
San Antonio, Texas

and

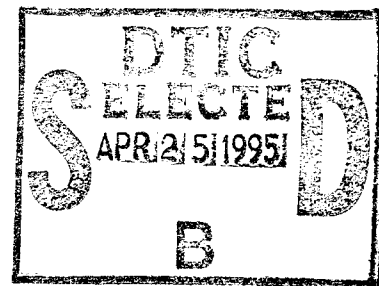
K. Randall Kohuth
General Pneumatics Corporation
Scottsdale, Arizona

Prepared by

Southwest Research Institute

Under Contract to

U.S. Army TARDEC
Mobility Technology Center-Belvoir
Fort Belvoir, Virginia



Contract No. DAAK70-92-C-0059

Approved for public release; distribution unlimited

March 1995

19950425 111

Disclaimers

The findings in this report are not to be construed as an official Department of the Army position unless so designated by other authorized documents.

Trade names cited in this report do not constitute an official endorsement or approval of the use of such commercial hardware or software.

DTIC Availability Notice

Qualified requestors may obtain copies of this report from the Defense Technical Information Center, Cameron Station, Alexandria, Virginia 22314.

Disposition Instructions

Destroy this report when no longer needed. Do not return it to the originator.

| REPORT DOCUMENTATION PAGE | | | Form Approved OMB No. 0704-0188 | |
|--|---|---|------------------------------------|----------------|
| Public reporting burden for this collection of information is estimated to average 1 hour per response, including the time for reviewing instruction, searching existing data sources, gathering and maintaining the data needed, and completing and reviewing the collection of information. Send comments regarding this burden estimate or any other aspect of this collection of information, including suggestions for reducing this burden, to Washington Headquarters Services, Directorate for Information Operations and Reports, 1215 Jefferson Davis Highway, Suite 1204, Arlington, VA 22202-4302, and to the Office of Management and Budget, Paperwork Reduction Project (0704-0188), Washington, DC 20503. | | | | |
| 1. AGENCY USE ONLY (Leave blank) | 2. REPORT DATE Mar 95 | 3. REPORT TYPE AND DATES COVERED Interim Jan 94 to Dec 94 | | |
| 4. TITLE AND SUBTITLE Natural Gas Liquefier for Vehicle Fuel | | 5. FUNDING NUMBERS DAAK70-92-C-0059; WD 20 | | |
| 6. AUTHOR(S) Owens, Edwin C. (SwRI) and Kohuth, K. Randall (GPC) | | | | |
| 7. PERFORMING ORGANIZATION NAME(S) AND ADDRESS(ES) Southwest Research Institute P.O. Drawer 28510 San Antonio, Texas 78228-0510 | | 8. PERFORMING ORGANIZATION REPORT NUMBER TFLRF No. 310 | | |
| 9. SPONSORING/MONITORING AGENCY NAME(S) AND ADDRESS(ES) Department of the Army Mobility Technology Center-Belvoir 10115 Gridley Road, Suite 128 Ft. Belvoir, Virginia 22060-5843 | | 10. SPONSORING/MONITORING AGENCY REPORT NUMBER | | |
| 11. SUPPLEMENTARY NOTES Primary funding was provided by the U.S. Department of Defense, Advanced Research Projects Agency, Arlington, Virginia. | | | | |
| 12a. DISTRIBUTION/AVAILABILITY STATEMENT Approved for public release; distribution unlimited | | | 12b. DISTRIBUTION CODE | |
| 13. ABSTRACT (Maximum 200 words) This project was a continuation and refinement of a feasibility prototype natural gas liquefier that had been designed, fabricated, and tested under a U.S. Department of Energy (DoE) Small Business Innovation Research (SBIR) contract. Extensive performance testing was conducted to characterize the natural gas liquefier refrigeration capability and to collect data for diagnostic purposes. Analysis of the effectiveness of the regenerator concluded that the current design would require substantial empirical iterations. The final prototype with a design target of 1,000 Watts (W) refrigeration was able to achieve only 400 W of refrigeration, projected to 550 W at a higher charge pressure. Recommendations are made for further testing, analysis, and correlation to achieve a better optimized regenerator design for a second generation prototype natural gas liquefier. | | | | |
| 14. SUBJECT TERMS Natural Gas Liquified Gas Liquefier | | | 15. NUMBER OF PAGES 82 | 16. PRICE CODE |
| 17. SECURITY CLASSIFICATION OF REPORT Unclassified | 18. SECURITY CLASSIFICATION OF THIS PAGE Unclassified | 19. SECURITY CLASSIFICATION OF ABSTRACT Unclassified | 20. LIMITATION OF ABSTRACT | |

FOREWORD

The physical effort reported herein was performed by General Pneumatics Corporation (GPC), Western Research Center, Scottsdale, Arizona. GPC performed as a subcontractor to Southwest Research Institute (SwRI), San Antonio, Texas, under Contract No. DAAK70-92-C-0059 with the U.S. Army TARDEC Mobility Technology Center-Belvoir (MTCB), Ft. Belvoir, Virginia. Funding was provided by the U.S. Department of Defense, Advanced Research Projects Agency, Arlington, Virginia. Mr. Thomas C. Bowen (AMSTA-RBFF) of MTCB served as the contracting officer's technical representative and monitor.

| | |
|----------------------|--|
| Accession For | |
| NTIS GRA&I | <input checked="checked" type="checkbox"/> |
| DTIC TAB | <input type="checkbox"/> |
| Unannounced | <input type="checkbox"/> |
| Justification | |
| By | |
| Distribution/ | |
| Availability Codes | |
| Dist. | Avail and/or Special |
| A-1 | |

TABLE OF CONTENTS

| <u>Section</u> | <u>Page</u> |
|---|-------------|
| SOUTHWEST RESEARCH INSTITUTE (SwRI) ASSESSMENT OF THE APPENDED REPORT BY GENERAL PNEUMATICS CORPORATION (GPC) | 1 |
| APPENDIX | |
| Natural Gas Liquefier for Vehicle Fuel, Final Report | 3 |

SOUTHWEST RESEARCH INSTITUTE (SwRI) ASSESSMENT OF THE APPENDED REPORT BY GENERAL PNEUMATICS CORPORATION (GPC)

The Stirling cycle refrigerator, developed during earlier Department of Energy (DOE) Small Business Innovation Research (SBIR)-funded work, was the focus of this project. General Pneumatics Corporation (GPC), under contract with Southwest Research Institute (SwRI), was to redesign the drive mechanism of the Stirling cycle refrigerator to improve mechanical reliability and to revise the system design to improve the cycle efficiency. The long-term objective for GPC is to develop a small, low cost natural gas liquefier that would be the basis for a home refueling system for liquefied natural gas-fueled vehicles.

The Ross drive mechanism was redesigned to eliminate the fatigue failures of the original flexure rods used to connect the pistons to the drive crankshaft. A revised linkage was developed and tested, and initial results show improvement in durability. While the rod failures have been eliminated, there appears to be several areas in which reliability may be a concern, such as in the piston seals and the bellows used to seal the crankcase. However, the mechanical reliability of the prototype appears to be substantially improved.

In order to improve the Stirling cycle efficiency of the refrigerator, much of the project focused on analysis of the effectiveness of the regenerator and other components within the heat exchange system, since these components have a large impact on overall efficiency. Most of GPC modeling was focused on the regenerator. It was concluded that the current regenerator design was only 1 percent ineffective and would require substantial empirical design iterations to improve this area.

The final prototype, without ancillary equipment ultimately necessary for operation, was able to provide 400 Watts (W) of refrigeration at the liquid methane temperature of 112°K, and was projected to achieve about 550 W at a higher charge pressure. This is substantially below the target of 1,000 W of refrigeration. The coefficient of performance (COP), which could theoretically reach 0.6 for this operating temperature, was only able to reach 0.16. This is much poorer performance and efficiency than hoped for, on the order of 5 percent overall efficiency

even without auxiliary equipment parasitic loads that would be necessary for a stand-alone system.

At the conclusion of the project, GPC has a functioning liquefier with improved mechanical reliability but without substantial improvement in operating efficiency from the prototype developed under Department of Energy-SBIR funding. It is unclear from their data whether substantial efficiency improvements are achievable for this type of system.

We would recommend a careful evaluation of market potential and requirements prior to further development efforts. While there appears to be potential markets for such a liquefier, such as condensation of boil-off from liquefied natural gas storage, the market the GPC envisions would be expected to be very sensitive to equipment cost and operating efficiency. Such an application analysis may have an impact on the size and performance requirements set for any follow-on development efforts.

Extensive detail and discussion are provided in the GPC technical report found in the appendix.

APPENDIX

Natural Gas Liquefier for Vehicle Fuel Final Report

Final Report

NATURAL GAS LIQUEFIER FOR VEHICLE FUEL

December 1994

Prepared for:

Southwest Research Institute
6220 Culebra Road
San Antonio, Texas 782338-5166

In response to:

Firm-Fixed Price Subcontract No. 93509
Under Government Contract No. DAAK70-92-C-0059

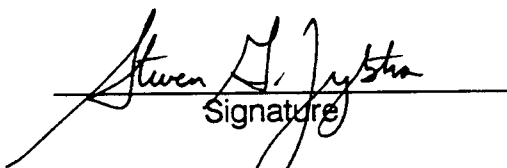
Prepared by:

General Pneumatics Corporation
Western Research Center
7662 E. Gray Road, Suite 107
Scottsdale, AZ 85260-6910
Ph. 602-998-1856
FAX. 602-951-1934

Principal Investigator
K. Randall Kohuth


Signature

Business Official
Steven G. Zylstra


Signature

Security Classification: Unclassified

CONTENTS

| | |
|---|----|
| EXECUTIVE SUMMARY | 1 |
| 1.0 INTRODUCTION | 4 |
| 2.0 PROJECT OBJECTIVES | 8 |
| 3.0 TECHNICAL APPROACH | 10 |
| 3.1 Stirling Machines | 10 |
| 3.2 Basic Mechanical Arrangement | 12 |
| 3.3 Computer Simulations | 13 |
| 3.4 Physical Description of Prototype NGL | 38 |
| 3.4.1 Drive Mechanism | 38 |
| 3.4.2 Heat Exchangers | 50 |
| 3.4.3 Cooler | 50 |
| 3.4.4 Regenerator | 51 |
| 3.4.5 Condenser | 56 |
| 3.4.6 Auxiliary Equipment | 57 |
| 3.4.7 System Operation, Control, and Safety | 58 |
| 4.0 TEST INSTRUMENTATION AND PROCEDURES | 60 |
| 5.0 TEST RESULTS | 67 |
| 6.0 CONCLUSIONS AND RECOMMENDATIONS | 74 |

EXECUTIVE SUMMARY

Natural gas offers many advantages as a vehicle fuel over gasoline, diesel, and alcohol fuels. These advantages include cleaner combustion with much less pollution, lower vehicle operating and maintenance costs, smoother, quieter operation, increased safety, and reduced dependency on imported oil. Studies by the Environmental Protection Agency, the Gas Research Institute, and others have shown that when the full cycle of energy production, distribution, and consumption is considered, natural gas vehicles are even less polluting than electric vehicles.

Liquid natural gas (LNG) is approximately 3 times denser than compressed natural gas (CNG) and is preferable as a vehicle fuel because of the savings possible in the size, weight and cost of the vehicle fuel tank and the extended vehicle range LNG can provide. LNG also offers a higher, more consistent methane content (critical to fuel quality control and engine performance) than typical CNG, and, as a liquid, allows faster refueling, since temperature-induced pressure increase inhibits complete CNG fast refilling. The major impediments to the use of natural gas as a vehicle fuel are the combined problems of lack of refueling facilities and limited vehicle driving range. General Pneumatics is developing a natural gas liquefier which addresses both of these problems. It produces LNG vehicle fuel directly from the established natural gas utility infrastructure which services more than 51 million residences and businesses in the U.S. And, since it liquefies the natural gas, it allows approximately 3 times more on-board fuel storage capacity than CNG. This provides almost the equivalent driving range as with conventional fuels.

The natural gas liquefier is intended as a practical, general-use fueling system for light-duty automobiles, small commercial fleets, and non-tactical military vehicles. The system can be connected to common natural gas distribution pipelines servicing private residences, small commercial establishments, or fleet refueling locations that are remote from larger, central refueling facilities. It can also be used to augment LNG storage and reliquefy boil-off at larger scale LNG fueling stations and storage sites to minimize emissions and stored LNG 'aging'.

The system under development is a Stirling cryocooler with a refrigeration capacity to produce approximately 8 liters of liquid natural gas per hour, which is adequate to fuel an average private automobile in an 8 hour period for a round trip of 300 km (186 miles). Priority is placed on achieving a minimum reliance on operator expertise or attention, and on establishing fail-safe tolerance of operator error, power loss, or component failure. The system design includes provisions for automated starting and for safe shutoff in the event of fueling completion, improper delivery hose connection, loss of power or natural gas flow, or out-of-limits operating temperatures, pressures, or speeds.

A feasibility prototype of a residential-sized natural gas liquefier was designed, fabricated, and tested under U.S. Department of Energy (DoE) Phase I and II Small Business Innovation Research (SBIR) programs. Further refinement and testing of this first prototype under the subject project was completed with funding from the U.S. Army contracted through the Southwest Research Institute. The next step will be to design, fabricate, and test a second-generation natural gas liquefier employing the knowledge gained from the feasibility prototype to develop a practical, high efficiency design. The

project will ultimately demonstrate the system operation, performance, and practicality for producing automotive fuel from pipeline gas. Emphasis will be placed on achieving simple fail-safe operation, low-maintenance reliability and long life, ruggedness, energy efficiency, and cost effectiveness for private, commercial, and military use.

The system design incorporates several features that minimize susceptibility to contamination, wear, and debris. These include use of the Ross drive linkage to minimize piston side forces, low operating speed and large-bore/small-stroke ratio for low piston seal rubbing speeds, low-friction piston seals to limit seal forces and wear, and location of bearings and piston seals away from extreme temperatures. The system is based on using low cost materials, fabrication methods, and components and avoiding the need for frequent servicing. It will make maximum use of standard commercially available parts, auxiliary equipment, and control components for economy of fabrication, operation, maintenance, and repair.

In a subsequent phase, after successful completion of the second-generation development and testing, it is planned to fabricate a preproduction liquefier for the purpose of conducting a natural gas vehicle demonstration project. A comprehensive test program will be conducted to gain experience in the utilization of the natural gas liquefier with a small representative fleet of LNG fueled vehicles. Three additional preproduction liquefiers will be built as part of the advanced development phase. One will be used for further bench testing at General Pneumatics' Western Research Center (GP WRC), another will be sent to the Southwest Research Institute for test and evaluation at their proposed LNG Vehicle Technology Center, and one will go to the AGA Laboratories for certification testing.

All the work described herein and for the proposed follow-on second-generation Stirling natural gas liquefier development was or will be performed at GP WRC in Scottsdale, Arizona. GP WRC was specifically established to research and develop cryorefrigerators, Stirling engines and refrigerators, and new approaches for thermal management and energy conversion. GP WRC has been in continuous operation since 1983 and has built up extensive experience in designing, fabricating, and testing small-scale Stirling machines. For the subject Stirling natural gas liquefier development, GP WRC has completed extensive marketing studies and developed a comprehensive business plan to anticipate the market potential, develop a commercialization strategy, and attract strategic partners.

1.0 INTRODUCTION

Pollution, global warming, and foreign oil dependency are providing the catalysts to develop alternatives to gasoline and diesel fuels for vehicles. Political, economic, and public pressures are mandating the production of clean-fueled vehicles in increasing numbers in the 1990's. Many consider natural gas to be the alternative fuel of choice.

Natural gas offers many advantages as a vehicle fuel over gasoline, diesel, and alcohol fuels. These advantages include cleaner combustion with much less pollution, lower vehicle operating and maintenance costs, smoother, quieter operation, increased safety, and reduced dependency on imported oil. Natural gas as a vehicle fuel can reduce reactive hydrocarbons and carbon monoxide by 90%, oxides of nitrogen by 50%, and can produce higher energy efficiencies in dedicated engines because of the fuel's 130 octane rating.

The primary constituent of natural gas, methane, is the simplest, most abundant hydrocarbon. It is non-toxic, non-carcinogenic, and poses no threat to surface or ground water. Because it has the highest hydrogen/carbon ratio (4/1) of any hydrocarbon, methane burns cleaner than any other fuel except hydrogen itself, which is much more difficult to contain and requires large amounts of energy (and associated pollution) to produce. Studies by the Environmental Protection Agency, the Gas Research Institute, and others have shown that when the full cycle of energy production, distribution, and consumption is considered, natural gas vehicles are even less polluting than electric vehicles.

Currently, natural gas is typically carried on a vehicle as high pressure (20 MPa) compressed gas. Liquid natural gas (LNG) is approximately 3 times denser than compressed natural gas (CNG) and is preferable as a vehicle fuel because of the savings possible in the size, weight and cost of the vehicle fuel tank and the extended vehicle range LNG can provide. For example, according to studies by the Houston Metropolitan Transit Authority, the full tank weights for the equivalent of 250 liters of diesel fuel are 250 kg for diesel, 290 kg for LNG, and 1150 kg for CNG. LNG also offers a higher, more consistent methane content (critical to fuel quality control and engine performance) than typical CNG, and, as a liquid, allows faster refueling, since temperature-induced pressure increase inhibits complete CNG fast refilling.

Alternative fuel vehicles (AFVs) suffer two principal shortcomings which limit their acceptance. First, the distribution infrastructure (fueling stations) to deliver fuel to the consumer is lacking. Second, the driving range of most AFVs falls far short of the

consumer's expectations. General Pneumatics is developing a natural gas liquefier which addresses both of these needs. It produces vehicle fuel directly from the established natural gas utility infrastructure which services more than 50 million residences and businesses in the U.S. Further, it liquefies the natural gas, allowing approximately 3 times more on-board fuel storage capacity compared to CNG. This provides almost the equivalent driving range as with conventional gasoline.

The natural gas liquefier is intended as a practical, general-use fueling system for light-duty automobiles, small commercial fleets, and non-tactical military vehicles. The system can be connected to common natural gas distribution pipelines servicing private residences, small commercial establishments, or fleet refueling locations that are remote from larger, central refueling facilities. It can also be used to augment LNG storage and reliquefy boil-off at larger scale LNG fueling stations and storage sites to minimize emissions and stored LNG 'aging'.

The system under development is a Stirling cryocooler with a refrigeration capacity to produce approximately 8 liters of liquid natural gas per hour. This is adequate to fuel an average private automobile in an 8 hour period for a round trip of 300 km (186 miles). Priority is placed on achieving a minimum reliance on operator expertise or attention, and on establishing fail-safe tolerance of operator error, power loss, or component failure. The system design includes provisions for automated starting and for safe shutoff in the event of fueling completion, improper delivery hose connection, loss of power or natural gas flow, or out-of-limits operating temperatures, pressures, or speeds.

For residential applications, the natural gas liquefier system will be installed where the vehicle to be fueled can be parked for 6 to 8 hours, such as a carport or driveway. Operation will be automated, requiring only that the operator connect the delivery hose to the vehicle, set a timer or select 'FILL', and press a 'START' button. The liquefier will automatically execute a start sequence and operate until the vehicle fuel tank is full, the set time elapses, a fault condition occurs, or the operator presses a 'STOP' button.

The only disadvantage of LNG as a vehicle fuel is the requirement for cryogenic temperature (112 K). This presents a significant challenge in designing a system which can be operated fail-safe by untrained individuals. It requires careful attention to safety issues, particularly in the design of the fuel transfer hose and coupling, and the control system. During the production design phase, the American Gas Association Laboratories, National Fire Protection Association, Underwriter Laboratories, safety engineers, and liability insurance providers will be consulted to address all safety issues.

A feasibility prototype of a residential-sized natural gas liquefier has been designed, fabricated, and tested under U.S. Department of Energy (DoE) Phase I and II Small Business Innovation Research (SBIR) programs. To date, \$550,000 was provided for this project by DoE and several hundred thousand dollars was invested by General Pneumatics. Further refinement and testing of this first prototype under the subject project was conducted with \$161,000 in funding from the U.S. Army contracted through the Southwest Research Institute. The follow-on phase will be to design, fabricate, and test a second-generation natural gas liquefier employing the knowledge gained from the feasibility prototype to develop a practical, high efficiency design. Emphasis will be placed

on achieving simple fail-safe operation, low-maintenance reliability and long life, a rugged design, energy efficiency, and cost effectiveness for private, commercial, and military use.

Subsequent to the proposed project, it is planned to install a preproduction liquefier at the U.S. Army Yuma Proving Ground (YPG) for a natural gas vehicle demonstration project. YPG will convert 4 light-duty passenger vehicles to operate on LNG and will conduct evaluations on vehicle fuel consumption, emissions, and maintenance. A comprehensive test program will be conducted in the utilization of the natural gas liquefier with this small representative fleet. The project will demonstrate the system operation, performance, and practicality for producing automotive fuel from pipeline gas.

Ultimately, General Pneumatics plans to develop a strategic alliance with a gas utility for the marketing, manufacturing and distribution of the natural gas liquefier. The small-scale liquefier will have widespread use in facilitating the advantages of LNG vehicles. With an initial target price of \$3,500 for the liquefier in volume production, an operating cost (including power and natural gas) of approximately \$0.75 per equivalent gallon of gasoline, and a low maintenance cost, the small-scale liquefier will be an attractive alternative to small-scale CNG units that are commercially available today.

2.0 PROJECT OBJECTIVES

The following tasks were to be performed by GPC under contract with SwRI toward the advanced development and demonstration of a Stirling natural gas liquefier for refueling light-duty vehicles.

1. Redesign the drive mechanism of the existing feasibility prototype to address flexure problems experienced during the U.S. Department of Energy SBIR project and apply experience gained through other Stirling projects at GPC.
2. Analyze and design an alternative regenerator and regenerator housing for comparative testing in the existing prototype liquefier.
3. Optimize the internal cooler and internal cold-end heat exchangers of the existing machine to improve its performance and efficiency.
4. Fabricate an alternative regenerator and regenerator housing for the prototype liquefier.
5. Fabricate new piece parts for drive mechanism, heat exchangers, and cold head, and reassemble the prototype liquefier.
6. Modify an existing test stand for mounting the prototype liquefier.
7. Conduct a test program on the prototype liquefier to evaluate the following performance parameters: motor power, coolant temperature, pressure cycle, cold end temperature at zero heat load, and maximum heat load for 110 K cold end temperature at various charge pressures and speeds.
8. Prepare quarterly letter progress reports (3).
9. Prepare a final report summarizing the effort undertaken, results obtained, and recommendations for follow-on development.

3.0 TECHNICAL APPROACH

3.1 Stirling Machines

The systems used for large-scale commercial liquefaction of gases do not scale down efficiently to the small size and intermittent duty cycle of the subject application. The type of machine most suitable for a small-scale natural gas liquefier is a Stirling cryorefrigerator. Stirling refrigerators offer the best potential efficiency and reliability for small cryocoolers. Progressively smaller, lighter Stirling cryocoolers have been developed over the past 40 years, principally for infrared night vision equipment and missile guidance systems requiring cooling in the range of 80 K. In competition with many other types of cryocoolers, including Vuilleumier, Linde-Hampson, Brayton, Claude, Gifford-McMahon, and Solvay, Stirling cryocoolers have emerged as the choice for small systems. For example, Linde-Hampson cryocoolers employ Joule-Thomson cooling by isenthalpic expansion of a high pressure gas through a nozzle to liquefy part of the gas. Linde-Hampson cryocoolers have typically not been used for long-life operation due to problems with compressor lubrication and wear and nozzle clogging. Power efficiency is inherently low due to losses in compressing the gas to high pressure and in expanding it through a nozzle without work recovery.

Stirling machines may be used as prime movers, refrigerating systems, or heat pumps. The ideal Stirling cycle has the same thermodynamic performance as the Carnot cycle, which defines the maximum work efficiency possible between given maximum and minimum temperature limits. While both ideal cycles are impossible to achieve in practice, Stirling machines can be built to achieve up to 50 percent of the Carnot performance.

The basic elements of Stirling machines are an expansion space and a compression space which are coupled through heat input, heat rejection (cooler), and regenerative heat exchangers. The regenerator acts as a thermodynamic sponge which alternately transfers heat to or from a gaseous working fluid that passes cyclically between the expansion and compression spaces. Two pistons (or a piston and a displacer) reciprocate in cylinders synchronously but out of phase so that the working fluid shuttles cyclically from one space to the other. The total working space volume and pressure also vary from maximum to minimum as the pistons cycle. The expansion space piston (or displacer) leads the compression space piston by about 90 degrees. Compression occurs when the working fluid is mostly in the compression space. Similarly, expansion occurs when the working fluid is mostly in the expansion space. Heat is alternately absorbed into the expansion space and rejected from the compression space.

For system compactness and efficiency, the working fluid is pressurized to as high a charge pressure as is structurally practical and safe. The most thermodynamically efficient Stirling working fluid is hydrogen, but safety and containment problems make it unsuitable for the subject application. The chosen working fluid, helium, offers the next best performance in terms of system power density and efficiency. A charge pressure of 2 MPa with a peak cycle pressure of 4 MPa at an operating speed of 16.7 Hz (1000 rpm) was determined to be optimum for overall system efficiency and practicality.

3.2 Basic Mechanical Arrangement

There are various forms of Stirling refrigerators, including kinematic (mechanically driven), free-piston, and pulse tube.

Free-piston Stirling machines have no mechanical linkage to the compressor piston or the displacer. The compressor piston is driven hydraulically or inductively and it in turn drives the displacer pneumatically. While eliminating the need for bearings, this arrangement requires precise resonant tuning of the drive and the piston and displacer dynamics, which varies with changes in temperature, friction, viscosity, clearances, etc., and does not provide the power efficiency of a mechanically controlled Stirling machine.

Pulse tube cryocoolers are Stirling-like refrigerators in which a pressure wave in a tube substitutes for a moving mechanical displacer. They may be driven with a thermoacoustic wave generator, instead of a mechanical compressor, to have no moving parts. However, because they rely on irreversible heat transfer or expansion processes to generate the essential cycle phasing, pulse tube refrigerators are intrinsically less efficient and bulkier than conventional Stirling refrigerators.

In kinematic Stirling refrigerators, the cycle phasing is optimally controlled by the drive mechanism, which couples the expansion and compression pistons. This can produce more than 3 times as much refrigeration per unit of mass flow, power input, and size compared with relying on irreversible heat transfer or isenthalpic expansion processes for cycle phasing as in pulse tube refrigerators.

Non-rubbing magnetic or gas bearings, flexures, and close-tolerance clearance seals are desirable for long life, but are not without serious difficulties. They all require extremely high precision which increases the complexity and cost of the design, and are

very sensitive to debris, vibration damage, thermal and mechanical strains, and misalignments. Magnetic suspensions require highly complex control electronics. The low density and viscosity of helium require extremely tight clearances in gas bearings. Non-contacting seals allow leakage past pistons in proportion to the clearance gap cubed, which wastes power and lowers compression ratio, necessitating a larger cryocooler for a given refrigeration capacity.

For overall practicality, efficiency, and cost effectiveness, the subject natural gas liquefier is a kinematic Stirling machine which employs proven, oil-lubricated bearings and can be driven by a standard, low-cost, ac induction motor. A cross-sectional diagram of the feasibility prototype as refined under this contract is shown in Figure 1, and photographs of the hardware in its test stand are shown in Figure 2.

3.3 Computer Simulations

Stirling machines operate in practice in a much more complicated fashion than the idealized thermodynamic cycle. Practical machines are subject to a variety of parasitic losses including mechanical and fluid friction (bearings, seals, and pressure losses in heat exchangers, etc.), conduction losses (along the cylinder walls from the warm to cool region), convection and radiation heat transfer to the cool region, and a variety of losses peculiar to Stirling machines known as shuttle heat transfer and hysteresis losses. All of these losses can be accounted for in realistic simulations of practical machine performance using computer programs at General Pneumatics' Western Research Center (GP WRC). The GP WRC computer simulations can accommodate virtually all configurations of Stirling machines and heat exchangers.

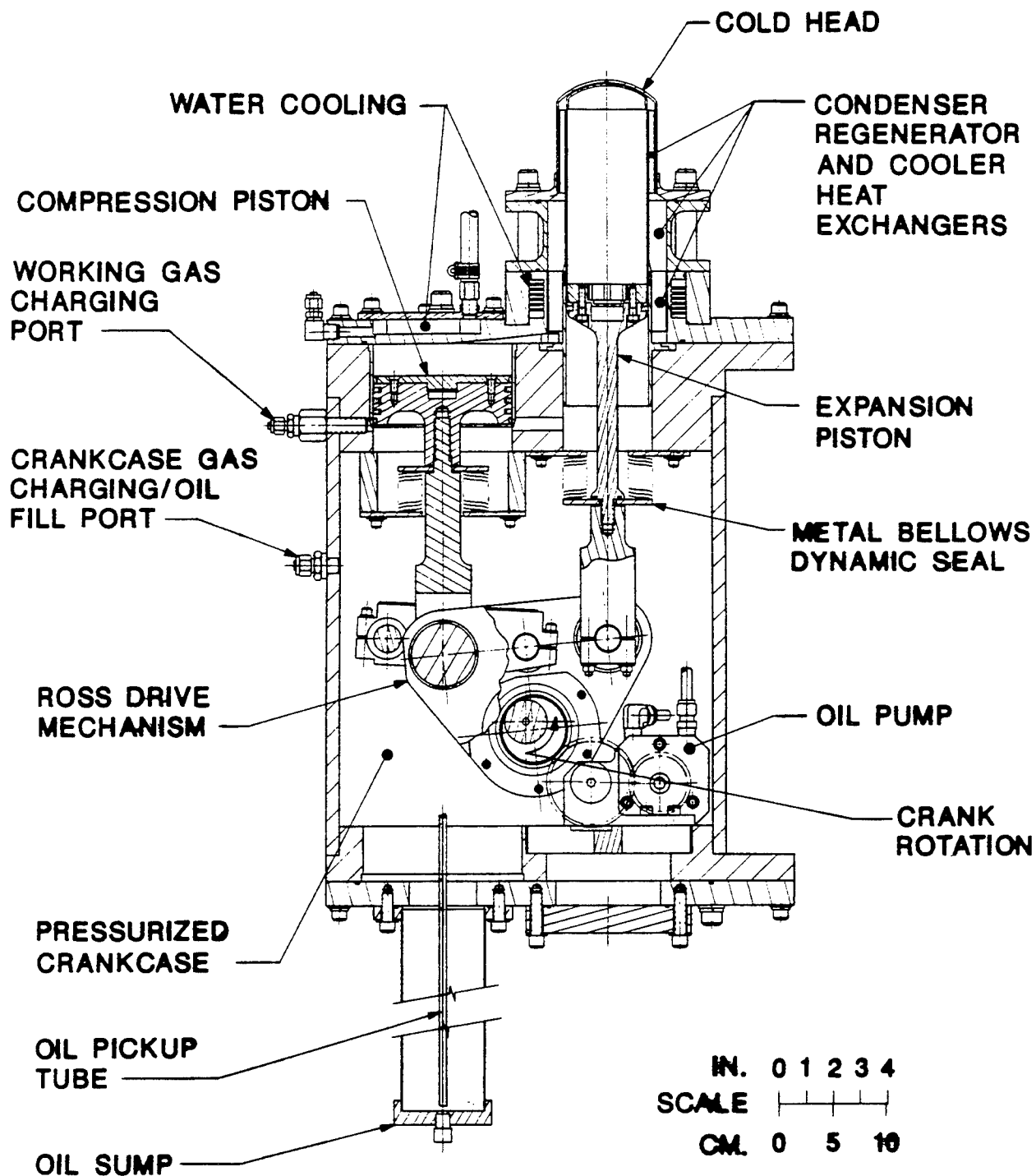


FIGURE 1a. PROTOTYPE ELECTRIC MOTOR DRIVEN STIRLING NATURAL GAS LIQUEFIER FOR VEHICLE FUEL

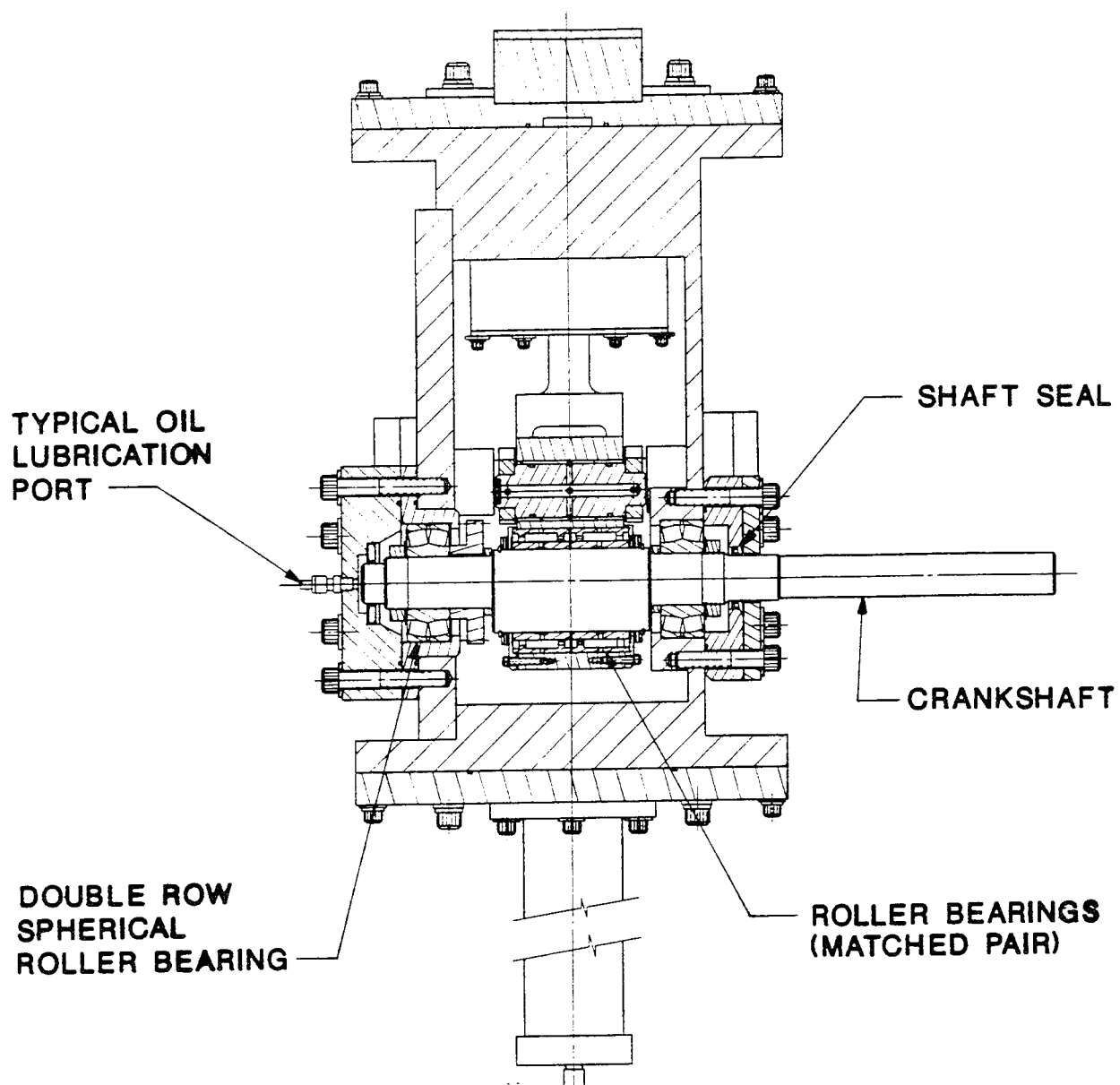
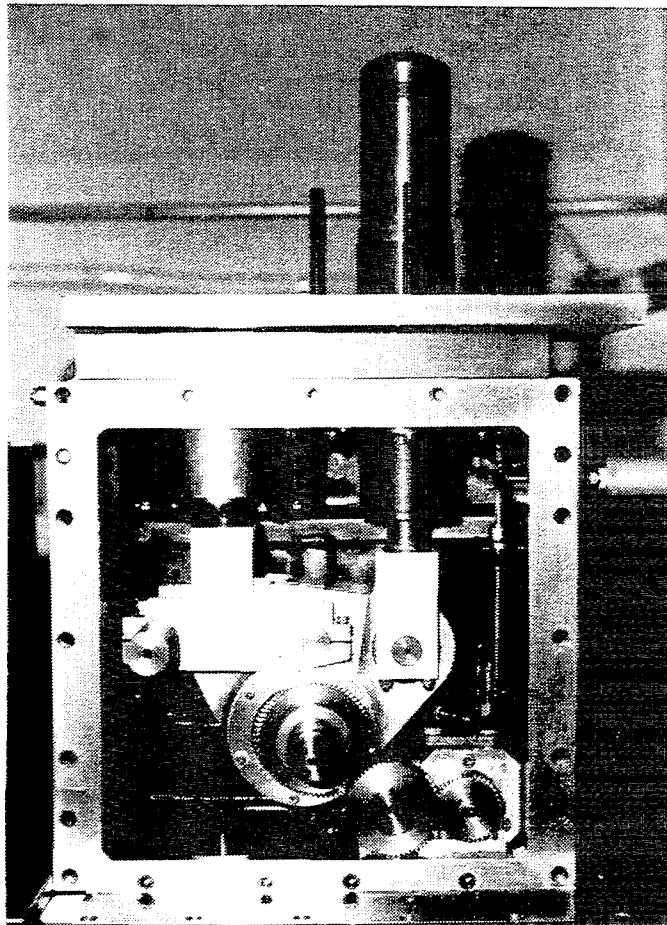
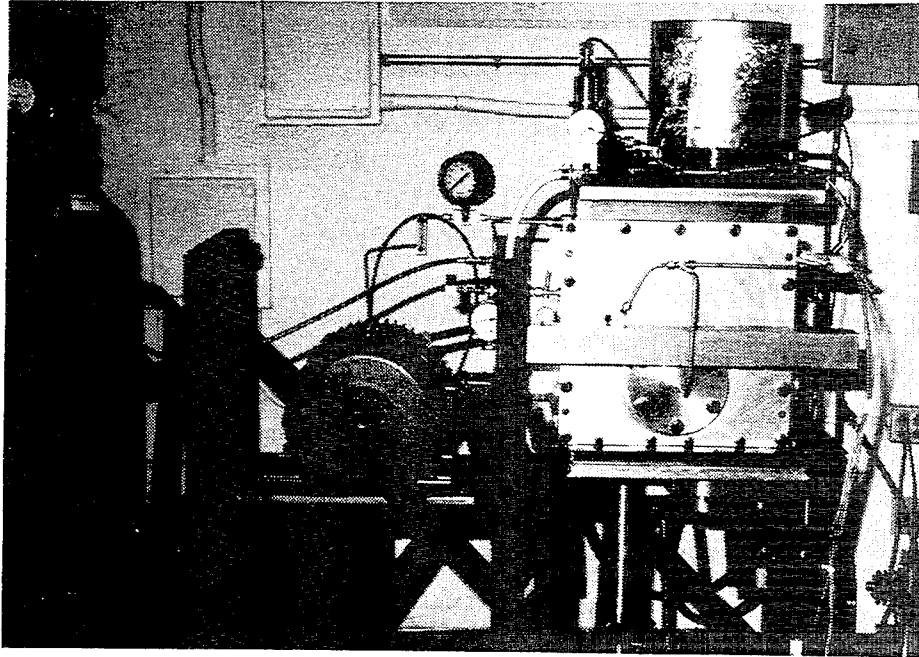


FIGURE 1b. PROTOTYPE NGL CROSS SECTION



**FIGURE 2. PROTOTYPE STIRLING NATURAL GAS LIQUEFIER
IN TEST STAND**

The Stirling simulation programs used by GP WRC were developed at the University of Calgary by Dr. G. Walker, R. Fauvel, and M. Weiss. The programs are based on the Martini second order, isothermal, decoupled corrections simulation technique which has proven effective in giving reasonable results within minimum computing time when compared with third order analysis techniques. The programs are written in Fortran 77 and adapted for use on computers using MS-DOS 2.0 or higher. They are completely modular to facilitate modification or addition of subroutines, and include extensive graphics of the effects of variables on Stirling machine performance, which are highly useful for design refinement and optimization.

The Stirling refrigerator simulation program is called CryoWeiss. The basic program requires definition of heat exchanger areas and volumes, compression and expansion space volume variation, mean gas pressure, and coolant and expansion cylinder temperatures. Gas properties such as pressure and temperature dependent parameters for viscosity, conductivity, heat capacity, and Prandtl number, are processed in a subroutine that allows different gases to be chosen as the working fluid. Heat exchange, fluid, and mechanical losses are handled in a separate subroutine that allows easy implementation of new analysis techniques and data. Several other subroutines correlate design configuration, drive, and dimensioning data into a general form for use in the basic program.

The performance of Stirling machines favors a low operating speed and high operating pressure rather than higher speed, lower pressure. The aerodynamic flow losses in Stirling machines are a function of the square of fluid velocity. Moreover, long

mechanism and seal operating life may be gained through relatively low speed operation. For these reasons emphasis was placed on machine operation in the speed ranges of 500 to 1500 revolutions per minute.

Starting with preliminary sizing analyses from the DoE SBIR Phase I of the development, in Phase II the geometrical, speed, and pressure parameters were varied in a series of iterative studies of the refrigerator design at cold and ambient temperatures of 100 K and 300 K to evolve the feasibility prototype design. This design was predicted to have a gross refrigeration capacity of 1.3 kW at liquid methane temperature (110 K) (about 1.0 kW net refrigeration capacity when external parasitics are taken into account) with a coefficient of performance of 0.22 corresponding to a power input requirement of 5.15 kW.

A copy of the CryoWeiss output is shown in Table 1. Various data were plotted to illustrate performance. The phased motion of the pistons, based on geometrical data from Table 1, causes volume and pressure variations as shown in Figure 3. Figure 4 is a plot of refrigeration capacity (heat lifted) as a function of speed and pressure. This plot illustrates that refrigeration is roughly linearly dependent on both speed and pressure. Based on this there is no obvious advantage in selecting one operating point over another except to operate at the highest pressure and speed practical to maximize refrigeration capacity (for a given size machine).

However, as seen in Figure 5, the power expended for refrigeration increases non-linearly with increasing speed. The ratio of refrigeration to required power input is defined as the coefficient of performance (COP). A COP map for various speeds and

TABLE 1 **CRYOWEISS STIRLING CRYOCOOLER SIMULATION**

STIRLING CRYOCOOLER SIMULATOR *CRYOWEISS* PC VERSION 1.1

CRYOCOOLER DIMENSIONS AND PARAMETERS

CRYOCOOLER TYPE **TWO PISTON MACHINE**

| | |
|---|-----------|
| Expansion cylinder diameter: | 7.620 cm |
| Compression cylinder diameter: | 12.700 cm |
| Expansion piston end clearance: | 0.050 cm |
| Compression piston end clearance: | 0.050 cm |
| Expansion cap gap: | 0.010 cm |
| Expansion cap length: | 14.000 cm |
| Number of piston/displacer pairs: | 1. |
| Clearance volume, expansion cylinder: | 2.280 cc |
| Clearance volume, compression cylinder: | 6.334 cc |

COOLER **TRAPEZOIDAL GROOVE**

| | |
|---------------------------|----------|
| Number of grooves / cyl.: | 300. |
| Length of grooves: | 5.350 cm |
| Depth of grooves: | 1.370 cm |
| Groove tip width: | 0.030 cm |
| Groove root width: | 0.030 cm |

CONNECTING DUCTS

| | |
|----------------------------------|-----------|
| Hydraulic diameter (conn. duct): | 2.000 cm |
| Length of conn. duct: | 5.000 cm |
| Number of conn. ducts / cyl.: | 1. |
| Dead volume / cyl. : | 50.000 cc |

REGENERATOR **WIRE MESH**

| | |
|--------------------------------|--|
| O.D. of regenerator: | 11.100 cm |
| I.D. of regenerator: | 7.680 cm |
| Length of regenerator: | 6.350 cm |
| Number of regenerators / cyl.: | 1. |
| Screen wire diameter: | 0.005 cm |
| Fill factor (fraction): | 0.350 |
| Surface area / volume: | 150.000 cm ² /cm ³ |
| Mesh density (strands per cm): | 89.127 |

FREEZER

TRAPEZOIDAL GROOVE

| | |
|---------------------------|----------|
| Number of grooves / cyl.: | 200. |
| Length of grooves: | 7.300 cm |
| Depth of grooves: | 0.500 cm |
| Groove tip width: | 0.030 cm |
| Groove root width: | 0.030 cm |

DRIVE SYSTEM

ROSS YOKE

| | |
|--|----------------|
| Exp. cylinder connecting rod length,(r6): | 10.000 cm |
| Comp. cylinder connecting rod length,(r5): | 6.000 cm |
| Crank length,(r2): | 1.000 cm |
| Comp. cyl. center to shaft center,(xe): | 7.620 cm |
| Exp. cyl. center to shaft center,(xf): | 7.620 cm |
| Free link length,(r3): | 7.620 cm |
| Swing link length,(r4): | 12.700 cm |
| Horizontal position of pivot,(a): | 12.700 cm |
| Vertical position of pivot,(b): | 7.620 cm |
| Comp. cyl. yoke arm length,(l3): | 10.770 cm |
| Comp. cyl. yoke arm angle,(phi3): | 45.000 degrees |
| Exp. cyl. yoke arm length,(l3') | 10.770 cm |
| Exp. cyl. yoke arm angle,(phi3'): | 45.000 degrees |
| Stroke, expansion cylinder: | 2.835 cm |
| Stroke, compression cylinder: | 2.828 cm |
| Swept volume, expansion cylinder: | 129.309 cc |
| Swept volume, compression cylinder: | 358.243 cc |
| Maximum live volume: | 438.723 cc |
| Minimum live volume: | 58.062 cc |
| Cooler dead volume: | 122.299 cc |
| Regenerator dead volume: | 211.560 cc |
| Heater dead volume: | 24.180 cc |
| Total dead volume: | 358.040 cc |
| Vmax / Vmin (total working space) | 1.915 |

MISCELLANEOUS PARAMETERS

| | |
|--------------------------------------|---------------|
| Heat transfer multiplication factor: | 1.000 |
| Cooling water flow rate: | 0.200 l/s |
| Metal thermal conductivity: | 14.000 W/ m K |
| Leakage (fraction): | 0.000 |
| Mechanical efficiency: | 85. % |
| Average pressure: | 3.000 MPa |
| Engine speed: | 1000. rpm |

| | |
|-------------------------------------|----------------|
| Cooling water temperature: | 320. K |
| Freezer wall temperature: | 100. K |
| Velocity head in freezer: | 1.000 |
| Velocity head in cooler: | 1.000 |
| Velocity head in conn. ducts: | 1.000 |
| Expansion cylinder wall thickness: | 0.200 cm |
| Expansion cap wall thickness: | 0.200 cm |
| Regenerator housing wall thickness: | 0.200 cm |
| Maximum pressure: | 3.757 MPa |
| Minimum pressure: | 2.049 MPa |
| Pmax / Pmin: | 1.834 |
| Phase angle: | 85.000 degrees |

CURRENT OPERATING CONDITIONS:

| | |
|--------------------------|----------------------------------|
| ENGINE SPEED = 1000. RPM | AVERAGE GAS PRESSURE = 2.800 MPa |
| DEGREE INCREMENT = 1 | GAS TYPE: HELIUM |

| POWER REQUIREMENTS, Watts | | REFRIGERATION, Watts | |
|---------------------------|---------|----------------------|---------|
| BASIC | 4642.92 | BASIC | 1683.60 |
| FREEZER F.L. | 34.20 | REHEAT | 93.57 |
| REGEN.F.L. | 280.56 | SHUTTLE | 50.96 |
| COOLER F.L. | 62.43 | PUMPING | 1.93 |
| NET | 5020.12 | TEMP. SWING | 36.13 |
| MECH. FRIC. | 885.90 | CONDUCTION | 169.57 |
| ACTUAL | 5906.03 | FLOW FRIC. CR. | -174.48 |
| | | NET REFRIGERATION | 1331.43 |

INDICATED 'COP' 0.2652
 ACTUAL 'COP' 0.2254

| | | | |
|-----------------------------|-------|-----------------------|-------|
| COLD METAL TEMP. (K): | 100.0 | EXP. TEMP.DIFF. (K): | 5.1 |
| EFF. EXP. SP. TEMP. (K): | 94.9 | COMP. TEMP.DIFF. (K): | -31.9 |
| COOLING WATER TEMP. (K): | 324.6 | | |
| EFFEC. COMP. SP. TEMP. (K): | 356.2 | | |

VOLUME AND PRESSURE VARIATION

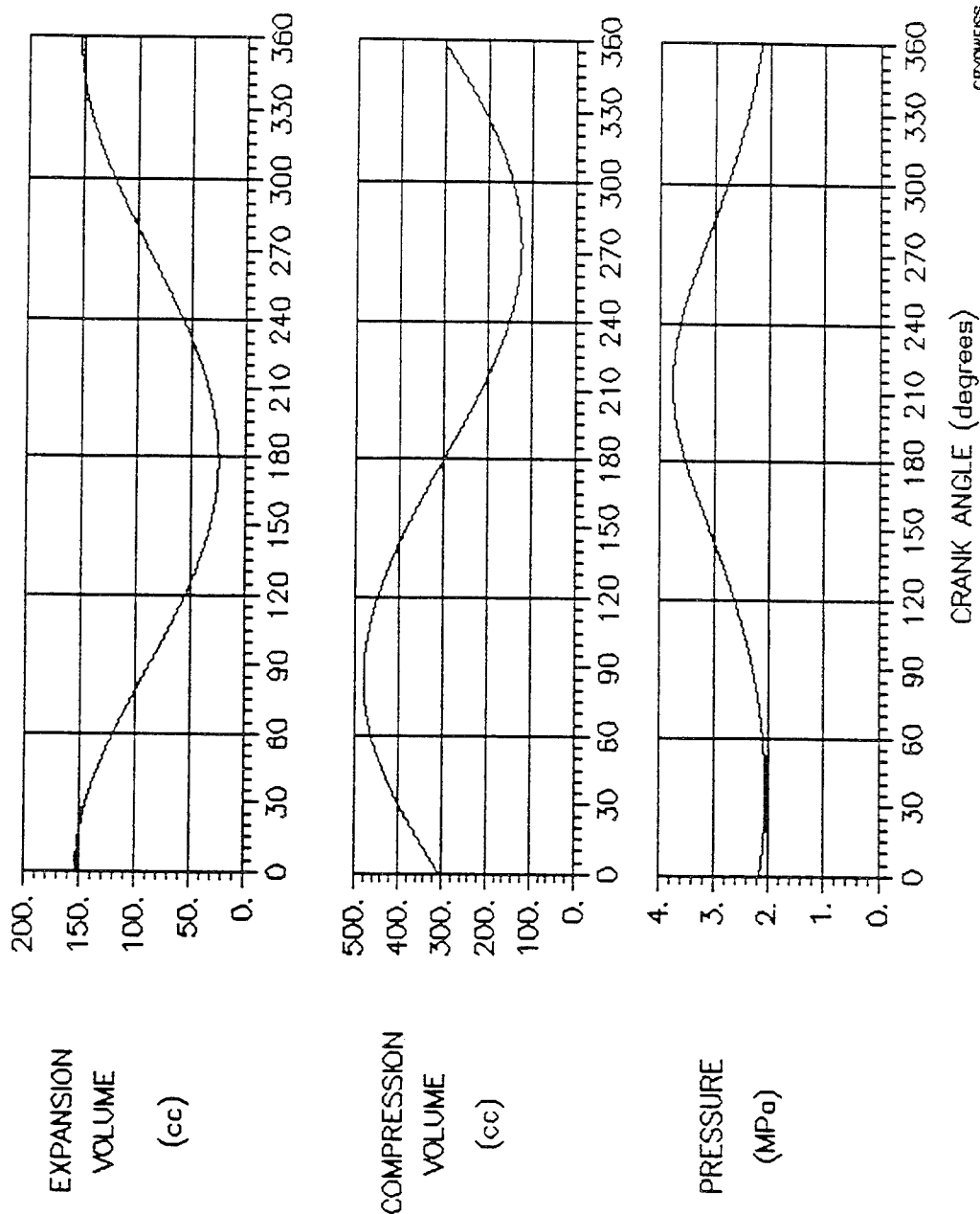
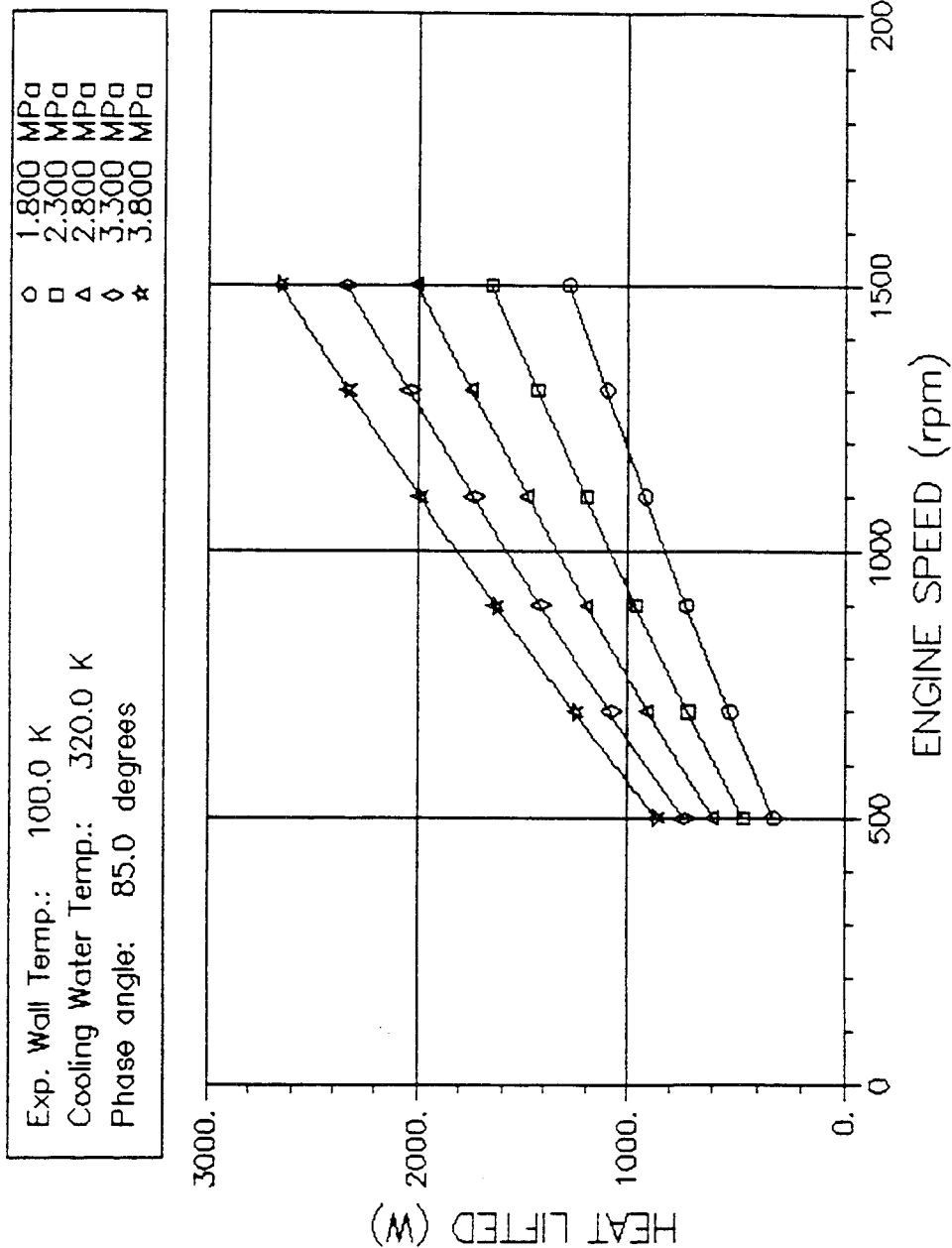


FIGURE 3. VOLUME AND PRESSURE VARIATION OF NGL

HEAT MAP

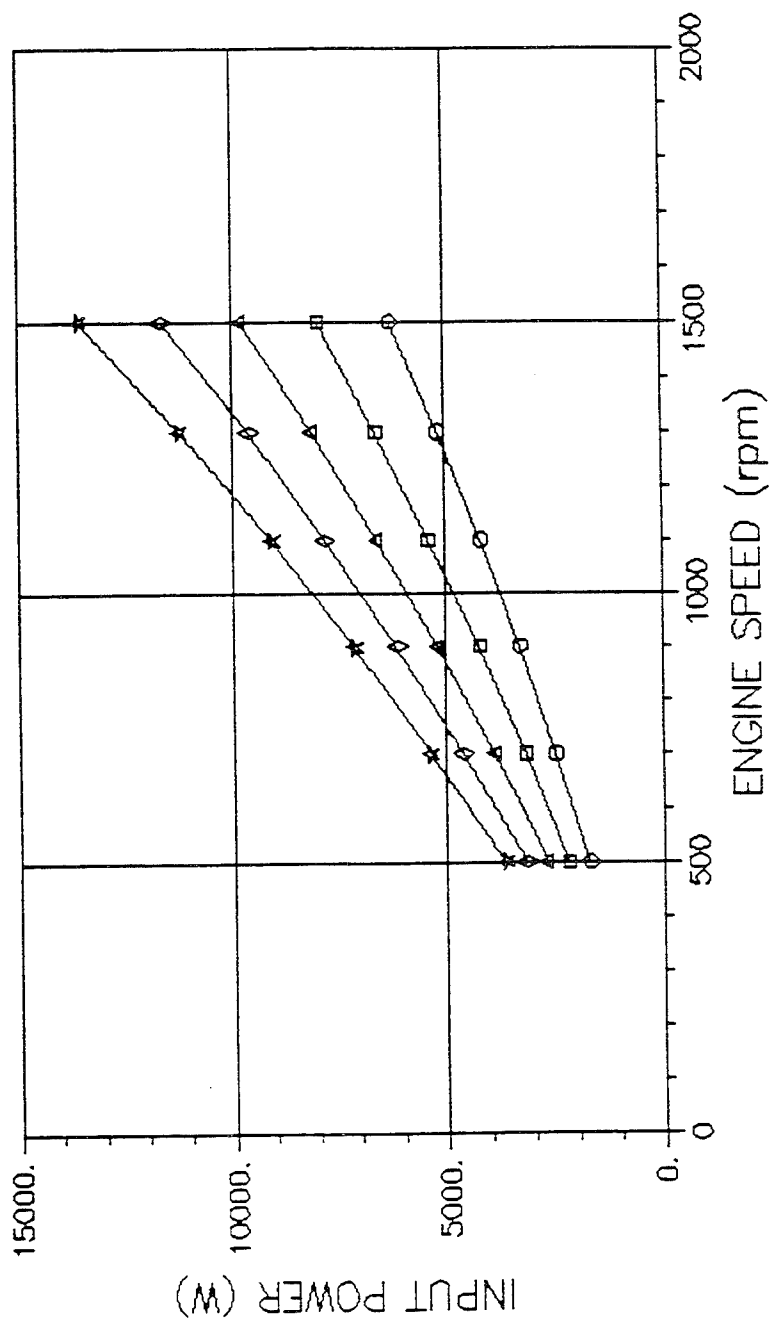


CRYOWESS ver. 1.1

FIGURE 4. HEAT MAP

POWER MAP

| | | | |
|----------------------|--------------|---|-----------|
| Exp. Wall Temp.: | 100.0 K | ○ | 1.800 MPa |
| Cooling Water Temp.: | 320.0 K | □ | 2.300 MPa |
| Phase angle: | 85.0 degrees | △ | 2.800 MPa |
| | | ◇ | 3.300 MPa |
| | | ★ | 3.800 MPa |



CRYOWESS ver. 1.1

FIGURE 5. POWER MAP

pressures is shown in Figure 6. The map shows declining performance at the higher speeds. For the targeted charge pressure of 2.0 MPa, which corresponds to a mean pressure of about 2.8 MPa, the optimum COP is shown to occur at about 800 rpm. However, a baseline design speed of 1000 rpm was chosen to allow margin for testing over a range of speeds.

The resulting pressure-volume cycles predicted by CryoWeiss for the NGL are shown in Figure 7. The work required to drive the thermodynamic cycle is the integral product of pressure and total-volume over the entire cycle and is represented by the area enclosed by the pressure vs total-volume plot in Figure 7. The gross thermodynamic refrigeration produced per cycle is represented by the area enclosed by the pressure vs expansion-volume plot shown in Figure 7.

Based on test results during the DoE SBIR Phase II development, it was suspected that the NGL's regenerator was causing poor performance. One of the main objectives of the subject follow-on project was to improve regenerator performance as necessary. The first step in this process was to derive a more thorough analytic model of the existing regenerator than is provided by CryoWeiss.

The best available means for analytically modeling regenerator performance is the REGEN series of computer models developed by Dr. Ray Radebaugh and his colleagues at the National Institute of Standards and Technology (NIST). Numerous computer simulations were performed using the recently available REGEN 3.1 third-order simulation program. Some of the effort was due to learning a new program and much of the effort was in fine tuning the parameters which affect the accuracy of the numerical modeling.

C.O.P. MAP

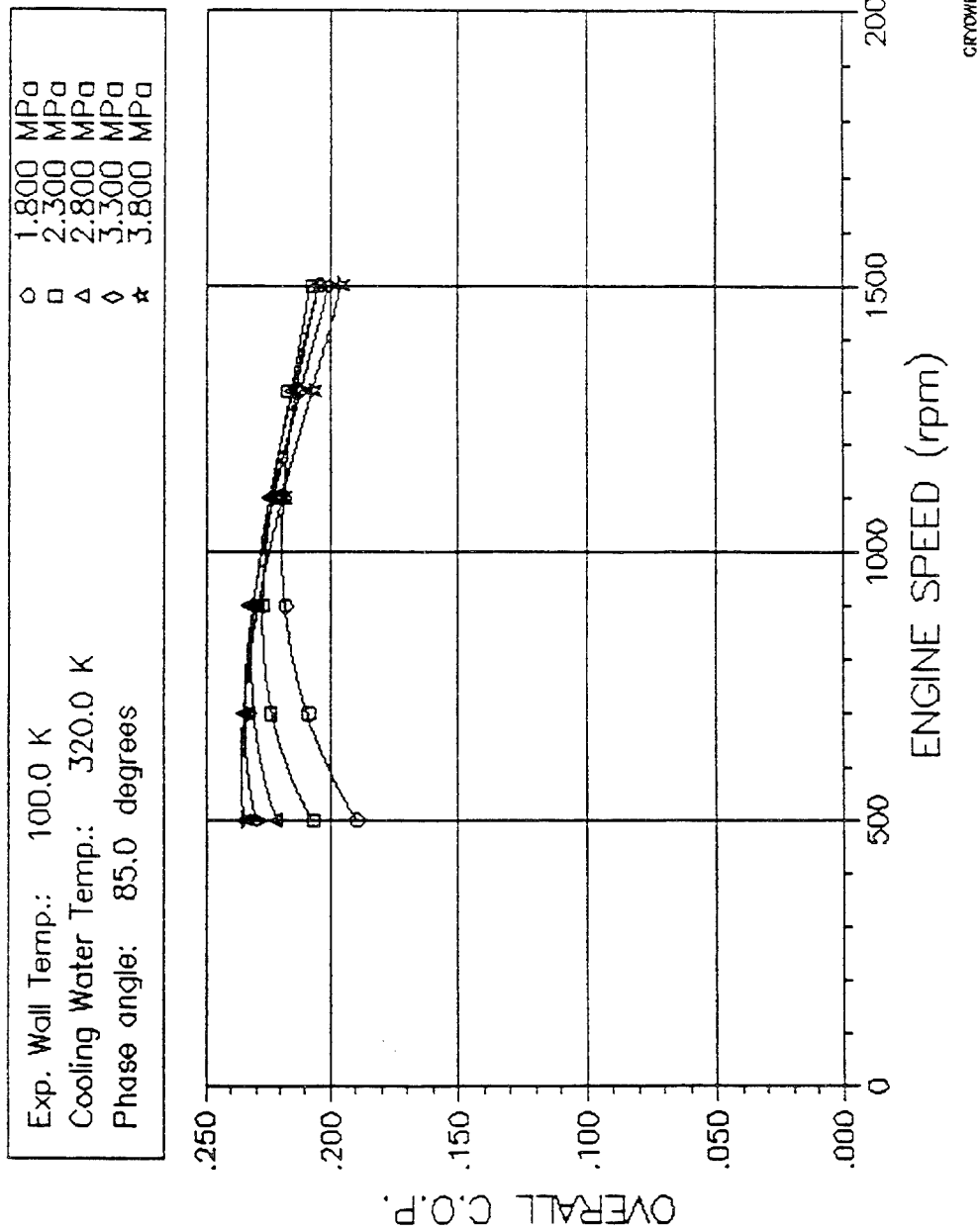


FIGURE 6. C.O.P. MAP

P - V DIAGRAM

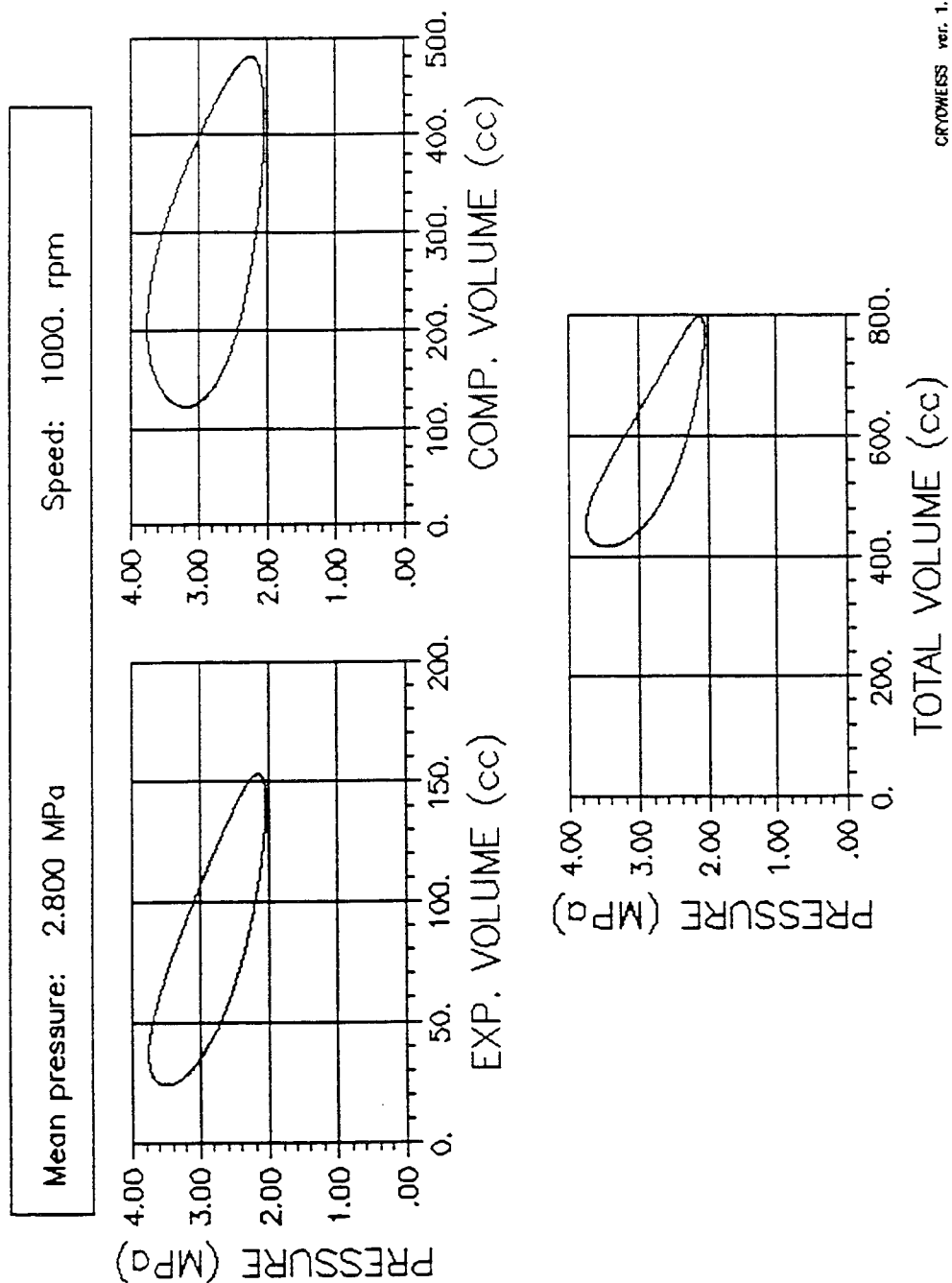


FIGURE 7. P - V DIAGRAM

The CryoWeiss simulations provided the basis for input to the REGEN 3.1 program. Mass fluxes were not explicitly listed in the CryoWeiss output but were obtained indirectly, as well as phasing information, from the gas flow distribution plot shown in Figure 8.

Over 100 input cases were run before arriving at a consistent quasi-steady-state solution. It would take well over 10,000 cycles to reach a steady-state solution. However, an acceptable quasi-steady-state solution was reached after 2000 cycles, in which the residual energy unbalance and difference terms had decayed to negligible values compared with the energy flow terms. A copy of the REGEN 3.1 output is listed in Table 2. The striking result of the simulation was that the regenerator effectiveness (one minus ineffectiveness) converged to 99 %. Therefore, the simulation indicated that the regenerator's performance was very good for the conditions under which the NGL is expected to operate.

TABLE 2 REGEN 3.1 INPUT/OUTPUT

| | |
|--|--------------------|
| REGEN3.1: Lahey version run on PC | 10/01/94 |
| REGEN3.1 \$Revision: 2.9 \$ \$Date: 93/10/25 17:52:26 \$ | |
| nrn=176 prtdev= 7 | |
| Input data read for a new case, newcas = 1 | |
| Area of the regenerator (m**2) | AREARG = 5.000E-03 |
| Reduction factor for matrix thermal conductivity | FUDGE = 1.000E-01 |
| Scale factor for volumetric heat capacity | FACTCP = 1.000E+00 |
| Correction for non-isothermal refrigeration | REFADJ = 1.000E+00 |
| Input temperature at left (warm side) (K) | GTP0 = 3.200E+02 |
| Normalized midpoint temperature | GTPNM = 5.000E-01 |
| Input temperature at right (K) | GTP1 = 1.000E+02 |
| Frequency of mass input (herz) | HERZ = 1.670E+01 |
| Hydraulic diameter (m) | HIDIAM = 9.430E-05 |
| Select real(IDEAL=0) or ideal(IDEAL=1) helium gas | IDEAL = 1 |
| Selects the geometry of the regenerator | IGEOM = 4 |

| | |
|---|---------------------|
| 1:Parallel plates, 2:Axial tube flow, | |
| 3:Transverse tube flow 4:Screens 5:packed spheres | |
| 6:Open tube 7:Use htc1 for heat transfer | |
| 8: User supplied function, userht, for heat transfer | |
| Selects the matrix material (for thermal properties) | MATERL= 1 |
| 1:stainles steel, 2:g-10, 3:nylon, 4:lead, | |
| 5:brass, 6:nickel, 7:GdRh, 8:Gd(0.6)Er(0.4)Rh, | |
| 9:Er(3)Ni, 10:ErNi, 11:ErNi(2), 12:ErAl(2), | |
| 13:Er(0.2)Dy(0.8)Ni(2), 14:Kapton, 15:Neodyminum | |
| 16:high purity Er(3)Ni, 17:Er(0.9)Yb(0.1)Ni , 18:Er(3)Co | |
| 19:use cvm0,cvm1 heat cap and tmcnd0, tmcnd1 conductivity | |
| Peak mass flux at left (kg/s) | MFLUX0= 6.900E-02 |
| Peak mass flux at right (kg/s) | MFLUX1= 6.900E-02 |
| Number of mesh intervals in regenerator | NRG = 30 |
| Initial pressure (Pa) | P0 = 2.600E+06 |
| Phase of mass flux at left (deg) | PHASE0 = 0.000E+00 |
| Phase of mass flux at right (deg) | PHASE1 = -4.200E+01 |
| Porosity | POR1 = 6.500E-01 |
| Length of regenerator (m) | XLENRG = 6.350E-02 |
| Input data which controls the numerical method | |
| Used to smooth gas temp when boundary velocity reverses | DECAY = 1.000E-02 |
| Convergence tolerance for temperature computation | EPSTP = 0.000E+00 |
| Convergence tolerance for velocity iteration | EPSUIT= 1.000E-05 |
| Factor to smooth velocity in matrix heat transfer | HTALP = 4.000E-02 |
| Factor to smooth velocity in matrix heat transfer | HTGAM = 2.000E+00 |
| Selects type of mass flow boundary condition at left | IBDRY0= 0 |
| Selects type of mass flow boundary condition at right | IBDRY1= 0 |
| Select constant matrix thermal conductivity | IGCOND= 0 |
| Select constant matrix thermal conductivity | IMCOND= 0 |
| Select porosity defined by USERPO function | IPOROS= 0 |
| Select porosity defined by USERAR function | IAREA = 0 |
| Selects direct or table driven properties computation | ITBDIR= 0 |
| Maximum number of iterations in each time step | ITTMAX= 2 |
| Mesh index where history data will be taken | |
| IXHIST= 1 15 30 | |
| Sets number of points where history data is taken | MUSHIS= 3 |
| Sets number of temp points in thermo tables | NTB =200 |
| Sets number of pressure points in thermo tables | NPB =200 |
| Lower pressure limit in thermo tables (Pa) | PBMAX = 4.500E+06 |
| Upper pressure limit in thermo tables (Pa) | PBMIN = 1.600E+06 |
| Select pressure correction to conserve mass | PRCORR= 1 |
| Lower temp limit in thermo tables (K) | TBMAX = 4.000E+02 |
| Upper temp limit in thermo tables (K) | TBMIN = 9.000E+01 |

```

..... Input data for newcas line
Length of run      (cycles)      (cycles)      CYCEND= 2000.000
Interval between output (cycles)      CYCOUT= 500.000
Interval between output of history plots (cycles)      CYCHIS= 10.000
Number of history samples per cycle      NDTHIS= 0
Number of time steps per cycle      NTSTEP= 300
Other output control:      nprint= 3 nplot= 0 bugprt= 0
----- END INITIAL INPUT DATA -----
..... Output at END CYCLE      at cycle= 2000.000 cpu time (s) = 3.15E+04
..... Output used to estimate convergence
Integral energy balance over the cycle (W)      ENGBAL= 6.714E-01
Difference in gas energy over the cycle (J)      ENGDIFF=-1.860E-03
Enthalpy+heat flux average across regenerator (W)      ENTAVE= 2.657E+02
Enthalpy+heat flux variation across regenerator (W)      ENTDF= 4.049E+00
Enthalpy+conduction at right side of regenerator (W)      ENTFLX= 2.688E+02
Average matrix temperature at midpoint      GTPNRM= 4.814E-01
Maximum difference in gas temp over cycle (K)      GTPDF= 8.096E-04
Maximum difference in matrix temp over cycle (K)      MTPDF= 8.088E-04
Average pressure over the cycle (Pa)      PAVE = 2.857E+06
Normalized pressure amplitude      PNORM = 3.143E-01
Ratio of maximum to minimum pressure at cold end      PRATIO= 1.915E+00
Maximum difference in pressure over cycle (Pa)      PRDF= -6.014E+00
Net energy passed to matrix during one cycle (W)      QINTW =-2.292E+00
..... Output at END CYCLE      at cycle= 2000.000 cpu time (s) = 3.15E+04
..... Output used to estimate ineffectiveness and cooling power
cZX Heat capacity of flowing gas (J/K)      CAPF = 6.802E+00
Heat capacity of regenerator matrix (J/K)      CAPR = 3.693E+02
Heat capacity of gas in void volume (J/K)      CAPV = 6.984E+00
Relative heat transfer per half cycle      CNTU = 3.258E+02
Average pressure drop in regenerator (Pa)      DELPAV= 3.065E+04
Maximum pressure drop over cycle (Pa)      DELPMX= 3.920E+04
Normalized maximum pressure drop      DLPMXN= 1.372E-02
Adjusted gross refrigeration power (W)      GRCADJ= 2.342E+03
Isothermal gross refrigeration power (W)      GRCOOL= 2.342E+03
Thermal flux from matrix at right side (W)      HTFLUX= 2.920E+00
Ineffectiveness      INEFCT= 1.060E-02
Normalization for ineffectiveness (W)      INEFNM= 2.508E+04
Mass of gas at the end of the cycle (kg)      MASS = 1.366E-03
Coefficient of performance      NTACOP= 2.676E-01
Adjusted net refrigeration power (W)      NTCADJ= 2.073E+03
Isothermal net refrigeration power (W)      NTCOOL= 2.073E+03
Phase angle of pressure drop rel to pressure (deg)      PDPPHS= 1.373E+01
Phase angle of compression vol rel to pressure (deg)      PHSCV = 1.137E+02
Phase angle of expansion vol rel to pressure (deg)      PHSEV =-1.083E+02

```


| | |
|---|-------------------|
| Phase angle of mass flow at right rel to left (deg) | PHSMAS= 4.200E+01 |
| Phase angle of mass flow at left rel to pressure (deg) | PHSPLM= 2.366E+01 |
| Phase angle of mass flow at right rel to pressure (deg) | PHSPRM=-1.834E+01 |
| Phase angle of T at midpoint rel to pressure at right (deg) | PHSTPM=-4.531E+01 |
| Phase angle of left end pressure rel to right (deg) | PLRPHS= 6.992E-01 |
| Maximum pressure over the cycle (Pa) | PMAX = 3.759E+06 |
| Minimum pressure over the cycle (Pa) | PMIN = 1.963E+06 |
| Portion of enthalpy flux due to pressurization (W) | PRLOSS= 1.017E-01 |
| Ratio of maximum to minimum pressure at hot end | PRTLFT= 2.006E+00 |
| Peak value of compression volume (m**3) | PTVMX1= 3.362E-04 |
| Peak value of expansion volume (m**3) | PTVMX2= 1.051E-04 |
| Additional(lost)warm end P-V work due to finite delta T (W) | PVLOSS=-3.248E+01 |
| Additional(lost)warm end P-V work due to delta P (W) | PVWKPR=-4.334E+02 |
| P-V work term at warm end with pressure correction (W) | PVWKOT=-7.747E+03 |
| P-V work term at the warm end (W) | PVWK0 =-7.314E+03 |
| P-V work term at the cold end (W) | PVWK1 = 2.342E+03 |
| Relative penetration of gas from left | RELLFT= 9.104E-01 |
| Relative penetration of gas from right | RELRHT= 7.418E-01 |
| Regenerator loss (W) | RGLOSS= 2.658E+02 |
| Entropy flux at warm end (W/K) | SFLUX0=-2.123E+01 |
| Alternate calculation of entropy flux at warm end (W/K) | SF0ALT=-2.203E+01 |
| Entropy flux at cold end (W/K) | SFLUX1=-2.192E+01 |
| Alternate calculation of entropy flux at cold end (W/K) | SF1ALT=-2.073E+01 |
| Entropy flux warm end (with delta P) (W/K) | SFLX0P=-2.259E+01 |
| Alternate calc entropy flux warm end(with delta P)(W/K) | SF0PAL=-2.338E+01 |
| Normalized gas temperature amplitude | TNORM = 1.134E-02 |

| Mesh index | mass flux pos average (kg/s) | mass flux pos peak (kg/s) | heat flux integral (W) | enthalpy integral (W) | enthalpy+heat integral (W) |
|------------|------------------------------|---------------------------|------------------------|-----------------------|----------------------------|
| 1 | 4.377E-02 | 6.900E-02 | 6.564E+00 | 2.584E+02 | 2.650E+02 |
| 7 | 4.268E-02 | 6.759E-02 | 8.988E+00 | 2.571E+02 | 2.661E+02 |
| 13 | 4.152E-02 | 6.569E-02 | 8.420E+00 | 2.573E+02 | 2.658E+02 |
| 19 | 4.082E-02 | 6.445E-02 | 7.593E+00 | 2.579E+02 | 2.655E+02 |
| 25 | 4.116E-02 | 6.477E-02 | 6.251E+00 | 2.588E+02 | 2.650E+02 |
| 31 | 4.374E-02 | 6.870E-02 | 2.920E+00 | 2.659E+02 | 2.688E+02 |

PRTSOL: timcyc= 2.000E+03 mass= 1.366E-03 pres= 2.507E+06

..... Input data for newcas line

| | | |
|---|------------------------------|------------------|
| Length of run (cycles) | (cycles) | CYCEND= 2003.000 |
| Interval between output (cycles) | | CYCOUT= 1.000 |
| Interval between output of history plots (cycles) | | CYCHIS= 3.000 |
| Number of history samples per cycle | | NDTHIS= 100 |
| Number of time steps per cycle | | NTSTEP= 300 |
| Other output control: | nprint= 3 nplot= 3 bugprt= 0 | |

GAS FLOW DISTRIBUTION

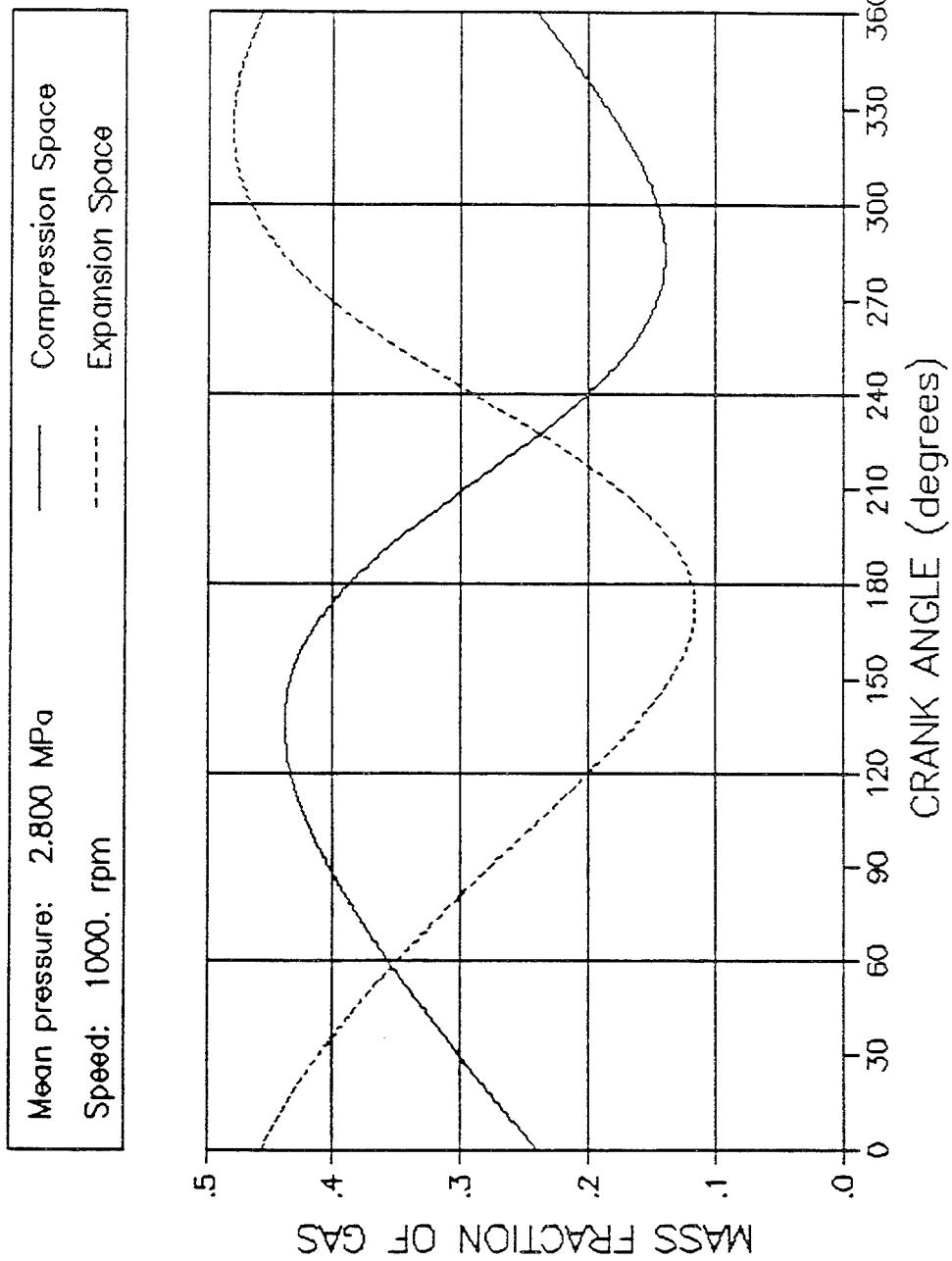


FIGURE 8. GAS FLOW DISTRIBUTION

Several aspects of the REGEN3.1 graphical output are interesting and allow insight into phenomenon not readily observable during testing. Figure 9 shows the mass flux through the regenerator warm end (FXO) and through the cold end (FXI) in relation to the pressure cycle. Mass flux through the cold end of the regenerator lags the mass flux through the warm end by about 42 degrees. Figure 10 is a plot of the volumetric specific heat of the gas (at 2.7 MPa cycle mean pressure) and matrix over the temperature range encountered. Because the matrix heat capacity is relatively large, the cyclic temperature swing of the matrix and gas at any given position along the regenerator can be small. The program does predict small temperature swings as shown by temperature histories at the regenerator warm (left) end and center ($x=L/2$) in Figures 11a and 11b. The maximum temperature swing is less than 5 K. The plots exhibit sharp cusps which occur at points of flow reversal. The horizontal flat areas and vertical drops in gas temperature shown in Figure 11a are a result of the constant temperature boundary condition imposed on the gas entering the warm end of the regenerator followed by flow reversal causing an abrupt drop in gas temperature at that location.

Although not used in the effectiveness calculations, pressure drop across the regenerator is also calculated by REGEN3.1. Figure 12 shows a plot of the pressure cycle and a plot of pressure drop across the regenerator. It is noted that the largest pressure drop (0.7 MPa) occurs when the pressure cycle is at a minimum and the density is lowest (volume rate is highest). Because of this flow loss, extra work is required to maintain the pressure cycle. This effect can be seen in the pressure-volume (P-V) diagram shown in Figure 13. The area enclosed by the large solid line P-V trace

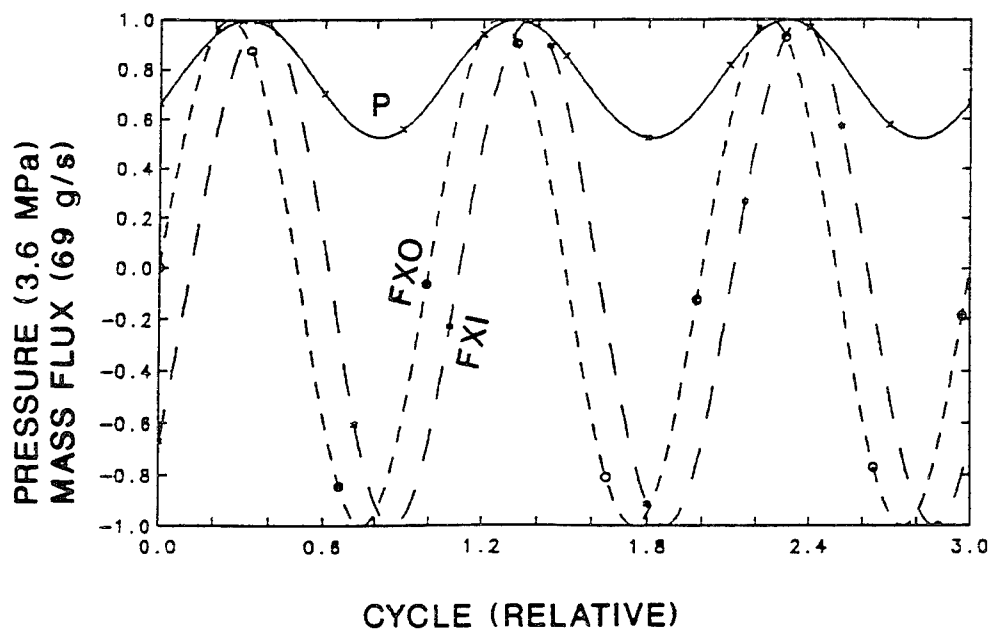


FIGURE 9. CYCLIC VARIATION OF PRESSURE (X) AND MASS FLUX AT WARM (O) AND COLD (*) ENDS OF REGENERATOR

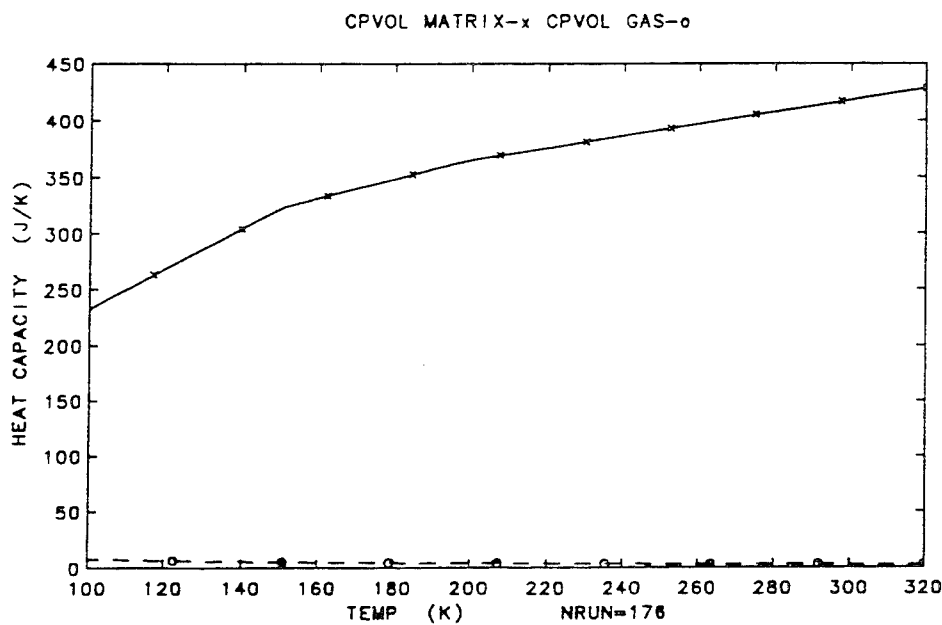


FIGURE 10. VOLUMETRIC SPECIFIC HEAT OF MATRIX (X) AND GAS (O) AT 2.7 MPa MEAN PRESSURE

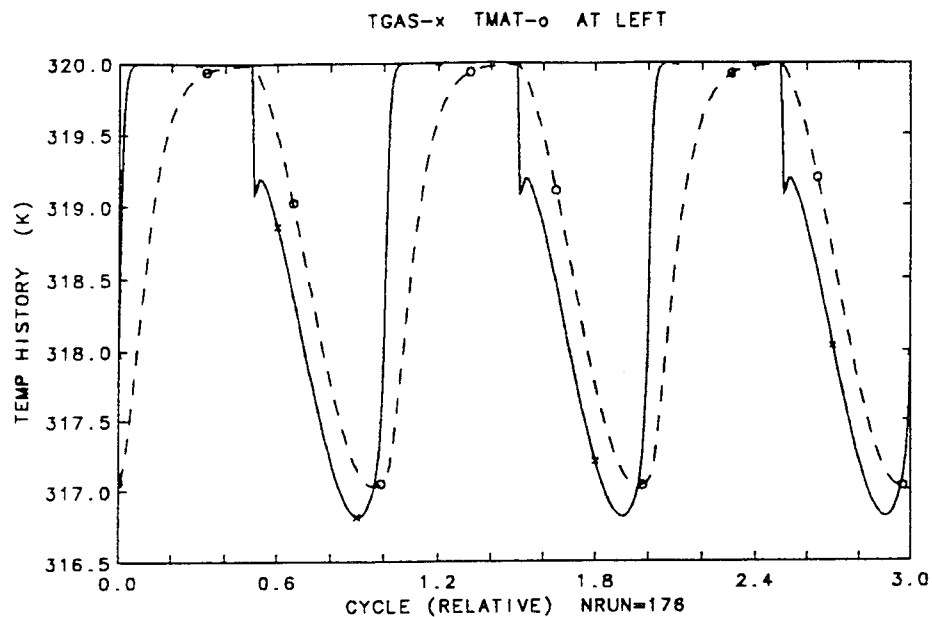


FIGURE 11a. TEMPERATURE HISTORY OF GAS AND MATRIX AT WARM END OF REGENERATOR FOR THREE REPRESENTATIVE CYCLES

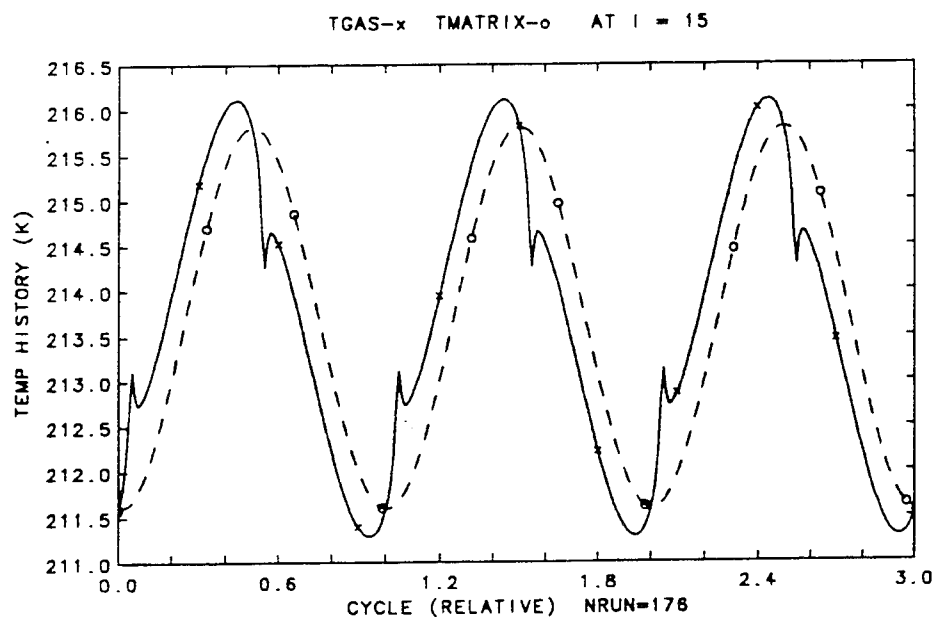
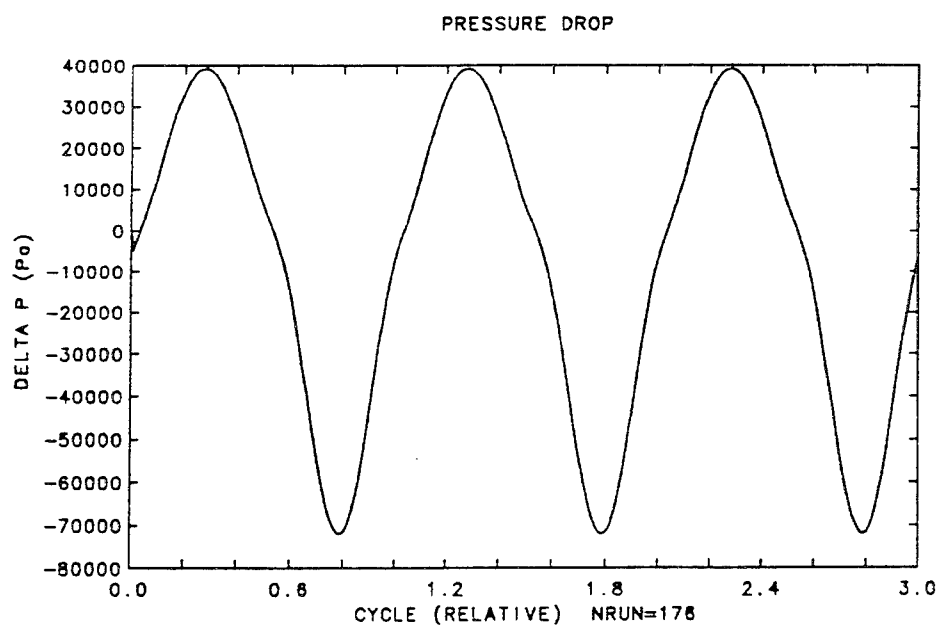
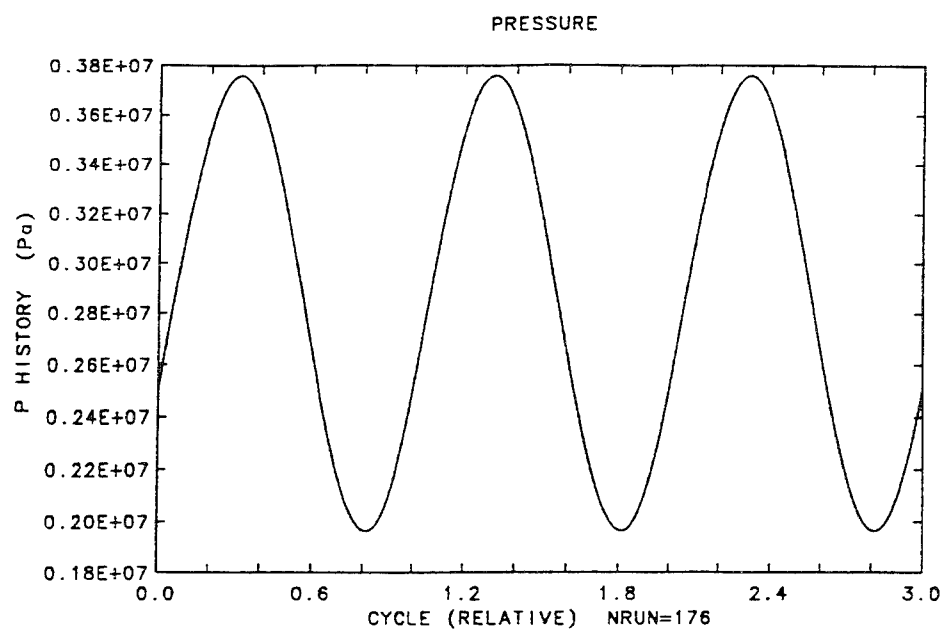
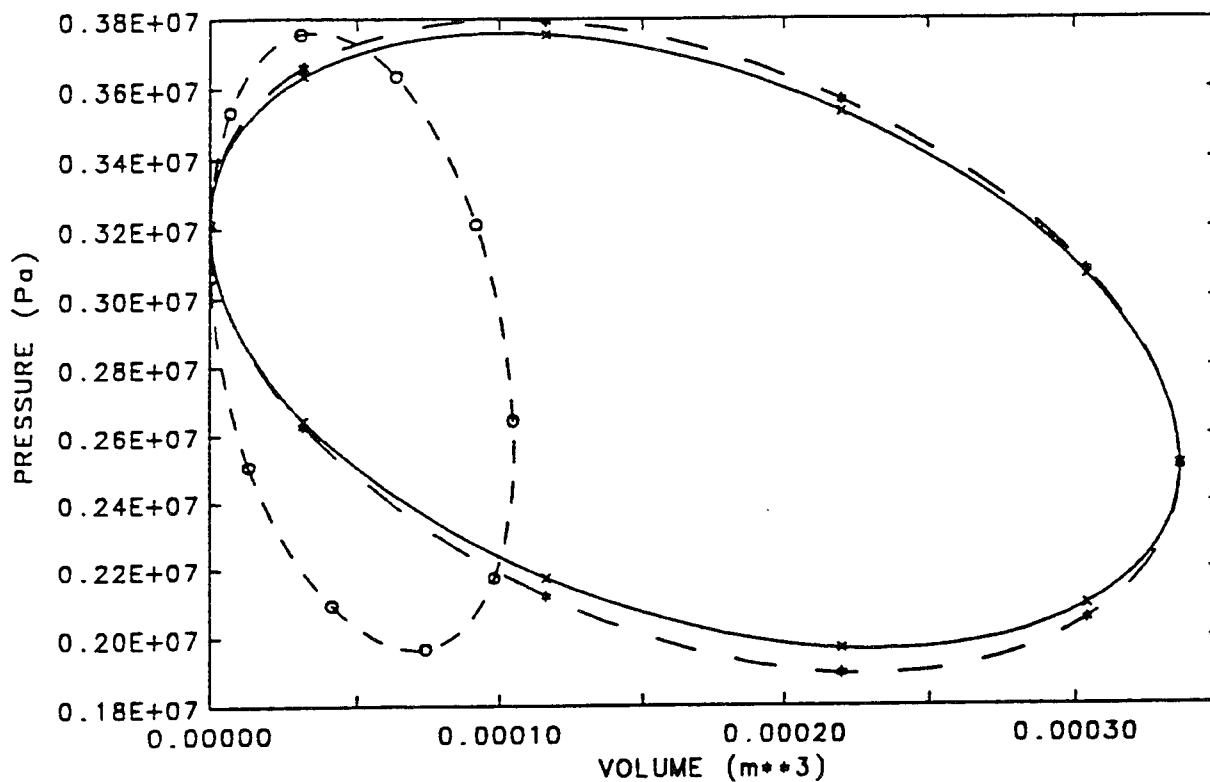


FIGURE 11b. TEMPERATURE HISTORY OF GAS AND MATRIX AT MIDDLE POINT OF REGENERATOR FOR THREE REPRESENTATIVE CYCLES



**FIGURE 12. CYCLE PRESSURE AND PRESSURE DROP
ACROSS REGENERATOR FOR THREE
REPRESENTATIVE CYCLES**



**FIGURE 13. PRESSURE-VOLUME DIAGRAMS FROM REGEN 3.1
 SHOWING EFFECT OF FLOW PRESSURE LOSS**

represents the work required per cycle, assuming no flow pressure loss through the regenerator, while the slightly larger dashed P-V trace indicates additional work required to overcome pressure drop through the regenerator. Quantitatively CryoWeiss (see Table 1) predicted a flow loss of 292 watts and REGEN 3.1 (see Table 2) predicted a flow loss of 433 watts.

Because REGEN3.1 predicted an effectiveness of 99 %, it was decided not to redesign and replace the regenerator. Although improvement may be possible, it was not realistic to analytically attempt to reduce a one percent ineffectiveness. Further refinement, if necessary, will require empirical iteration. Such refinement can be very time consuming and certainly beyond the scope of the subject project.

A dynamic analysis model of the drive mechanism and pistons was derived based on the Machinery Kinematics and Dynamics (MKAD) computer program. The program allows accurate modeling of the kinematics and mass properties of the system. Output from the model includes components positions, velocities, accelerations, forces, and reactions as a function of time. The combined pressure-induced and inertial loads used for sizing the structural members and bearings were determined using pressure-versus-crank-angle data from the CryoWeiss simulation program.

3.4 Physical Description of Prototype NGL

3.4.1 Drive Mechanism

Various forms of drive mechanisms were evaluated for the best suitability to accommodate the loads with the fewest bearings, minimum wear, and longest life. The mechanisms evaluated included conventional crank and connecting rods, rolling Scotch

yoke, rhombic drive, and Ross linkage. The conventional crank and the Scotch yoke were found to impose excessive side forces on the piston seals and guides, requiring lubrication to limit wear and prolong life. In Stirling machines residual oil on the cylinder wall can accumulate in and clog the regenerator matrix, leading to a loss in performance. Both the rhombic and Ross drives minimize side forces, but the rhombic drive involves more bearings and complexity. The Ross linkage was therefore preferred.

The Ross linkage is named after its inventor Andy Ross of Columbus, Ohio. The Ross linkage couples the pistons to the crankshaft so as to provide optimum phasing and near-straight-line motion with minimal side forces. The latter is especially important because piston side forces are the principal cause of seal wear and debris generation. The Ross linkage is advantageous because it:

- o Requires relatively small size and weight for a given swept volume;
- o Gives the pistons optimum phasing, smooth sinusoidal motion, and straight line travel;
- o Minimizes piston side forces, permitting use of oil-free piston seals, while minimizing seal wear to promote long operating life;
- o Facilitates a large bore/small stroke ratio for low piston seal rubbing speeds and short heat exchangers (regenerators and cooler) with minimal fluid pressure losses;
- o Allows closely spaced parallel cylinders which are easily connected with compact heat exchangers and minimum dead volume to promote high thermodynamic efficiency.

Previously, during the DoE SBIR Phase II program, it was attempted to use flexures to couple the piston rods to the Ross yoke. However, that approach was unsuccessful. Therefore, a major objective of the subject project was to completely redesign the drive mechanism but still retain the Ross linkage configuration. This led to all new drive mechanism components, including a core-hardened 4340 steel crankshaft for higher fatigue strength, as well as a new compression piston assembly. The major problem was corrected by replacing the 2 flexure elements with bearings. Rolling element bearings, previously used at locations where oscillatory motion is present, were replaced with journal bearings to prevent fretting wear. A pressurized oil circulation system was implemented to provide forced lubrication, instead of packed grease lubrication, to all of the bearings.

The revised Ross drive mechanism is shown assembled with pistons in Figures 14 and 15. The straight line motion of the Ross linkage facilitates the use of metal bellows behind the pistons to seal off the cylinders from the crankcase as can be seen in Figures 1, 15 and 16. This allows the use of proven oil-lubricated bearings sealed in an inert (helium) atmosphere at ambient temperature, while preventing lubricant vapors from entering into and condensing in the refrigerator cold working spaces. Since the prototype NGL is driven by a crankshaft which passes through the wall of the crankcase, a shaft seal is used. A spring-loaded rotary shaft seal from Bal-Seal company, suitable for a charge pressure of 300 psig, was mounted between retaining plates as shown in Figure 17. Both ends of the crankshaft are supported by large double-row spherical roller bearings as shown in Figure 18.

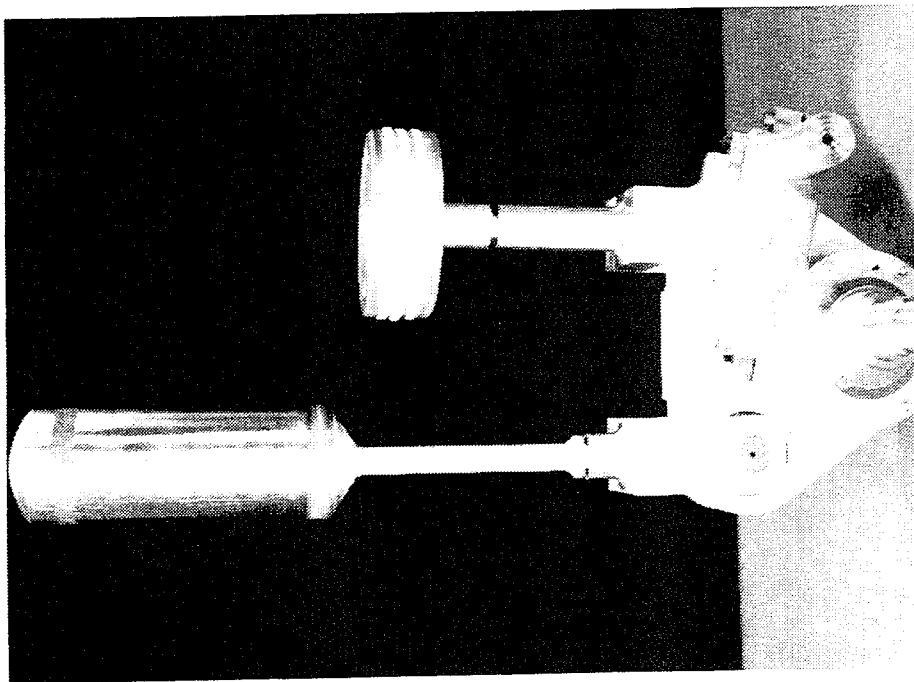


**FIGURE 14.
ASSEMBLED ROSS DRIVE
MECHANISM WITH PISTONS
ATTACHED BUT WITHOUT
BELLOWS SEALS**

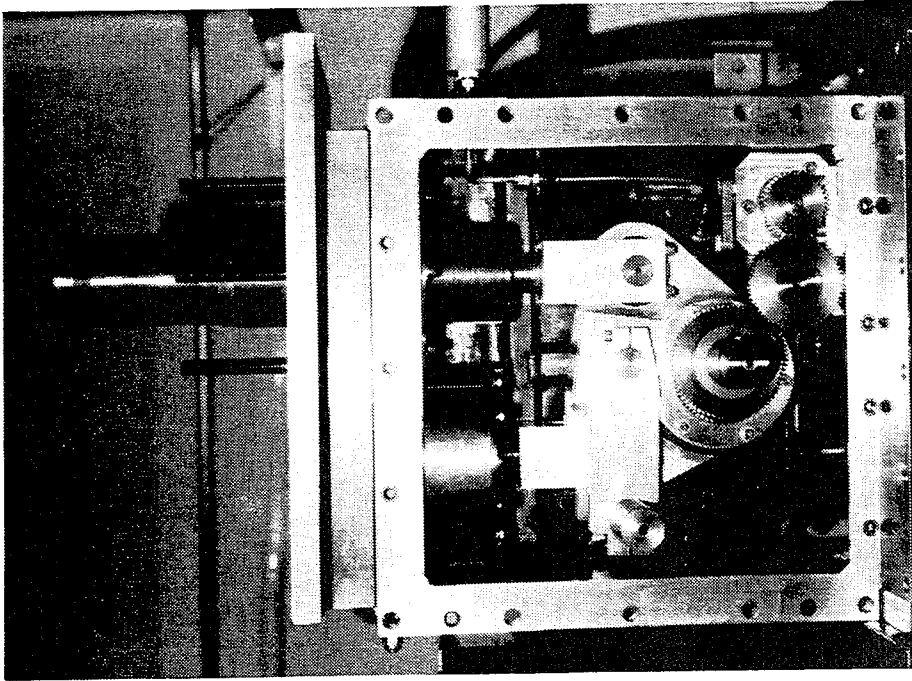


**FIGURE 15.
DRIVE MECHANISM, BELLOWS,
AND PISTONS INSTALLED IN
CRANKCASE**

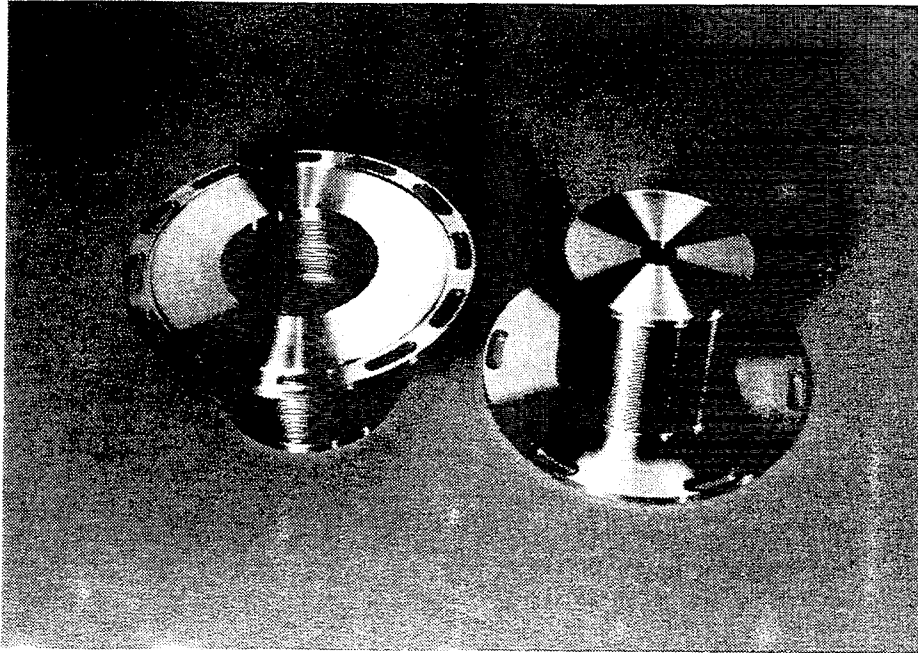


FIGURE 16. METAL BELLOWS DYNAMIC SEALS

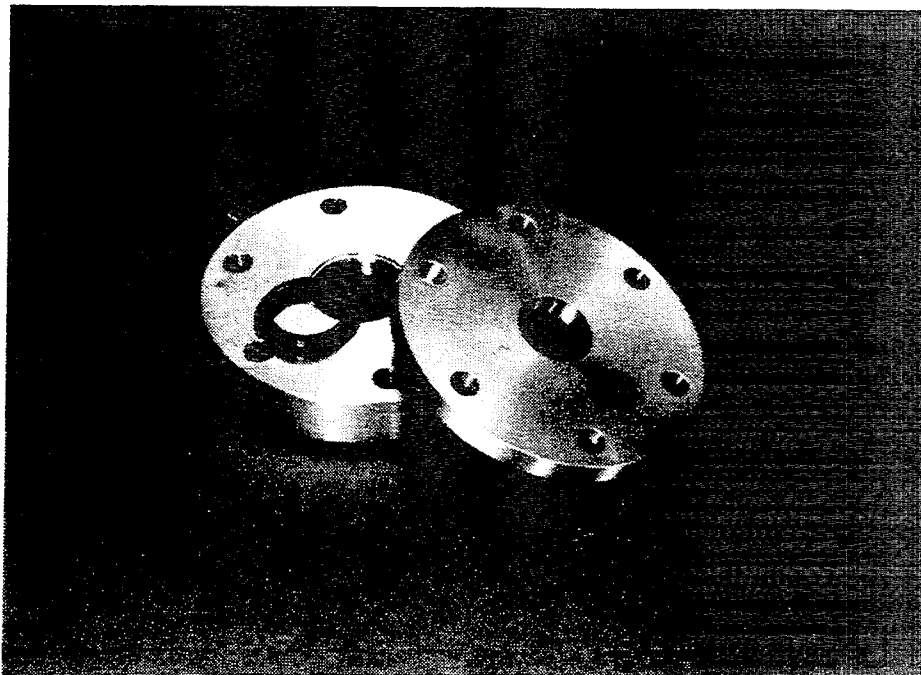


FIGURE 17. CRANKSHAFT SEAL AND ALUMINUM RETAINERS

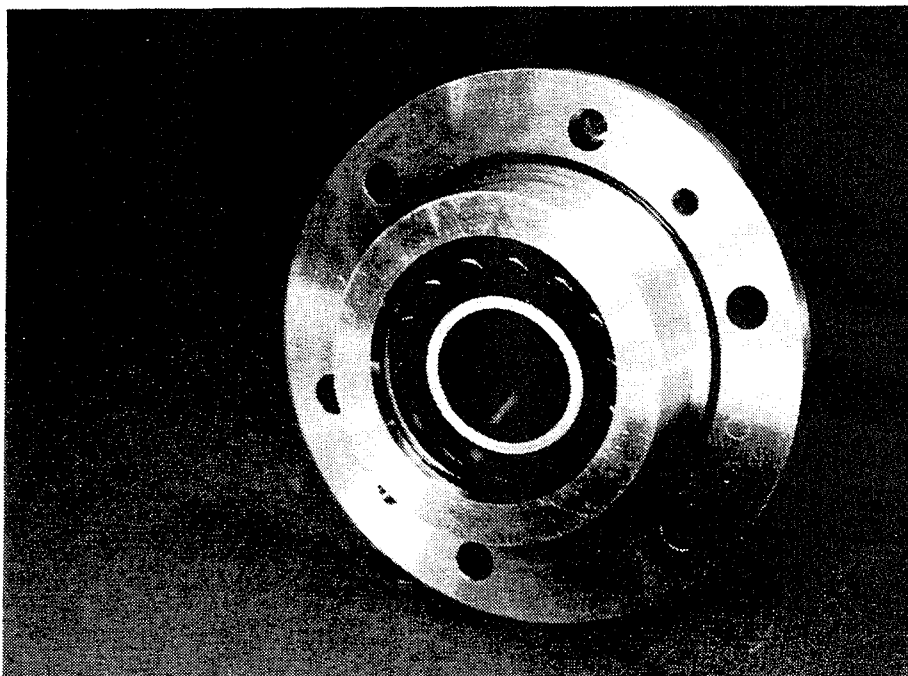


FIGURE 18. CRANKSHAFT END SUPPORT BEARING AND HOUSING

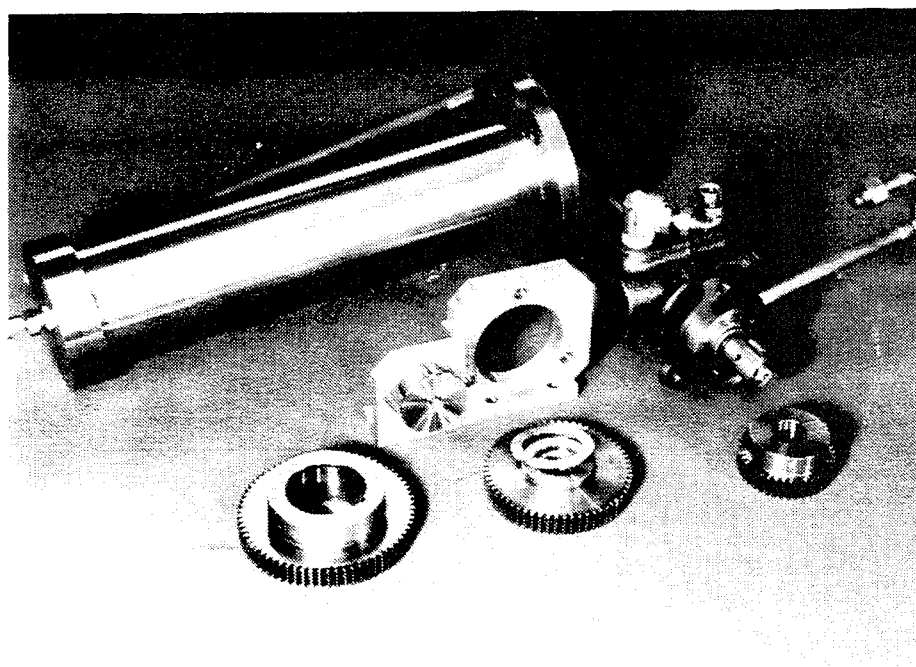


FIGURE 19. LUBRICATION SYSTEM COMPONENTS

All of the drive mechanism bearings are continuously lubricated with oil circulated by a gear driven oil pump located in the crankcase. Various oil lubrication system components are shown in Figure 19. Oil feed lines and filter are routed externally (see Figure 29) to the points where oil is delivered to ports feeding the swinglink pivot shaft and the crankshaft. Oil passages in these components allow oil to be delivered to bearings within the Ross drive yoke. The swinglink and various components of the Ross yoke are shown in Figures 20 and 21.

The expansion piston (Figures 14 and 22) is a long hollow thin wall 304 CRES structure to minimize heat conduction from the warm drive end to the cold region near the end of the piston. The expansion piston originally had a single lip seal at its base and guide ring at its top. To correct a possible contributor to the refrigeration deficiency observed in previous testing, a second, opposed, lip seal was added to the expansion piston base. The original lip seal minimizes piston blow-by while the opposing lip seal prevents blow-by gas from returning from the warm bellows space into the cold expansion space and thereby adding a parasitic heat load. Expansion piston blow-by gas is now returned to the warm compression space through an interconnecting passage between the bellows spaces and a flapper valve in the compression piston. The lip seals and guide ring are all made of Rulon® LD, a reinforced polytertrafluroethylene (PTFE teflon). This material has demonstrated excellent dry rubbing friction and wear characteristics in similar applications and wear testing.

The expansion piston reciprocates in a thin-wall 304 CRES liner treated with a low friction PTFE-impregnated nickel-phosphorus plating called NiCoTef®. The piston is

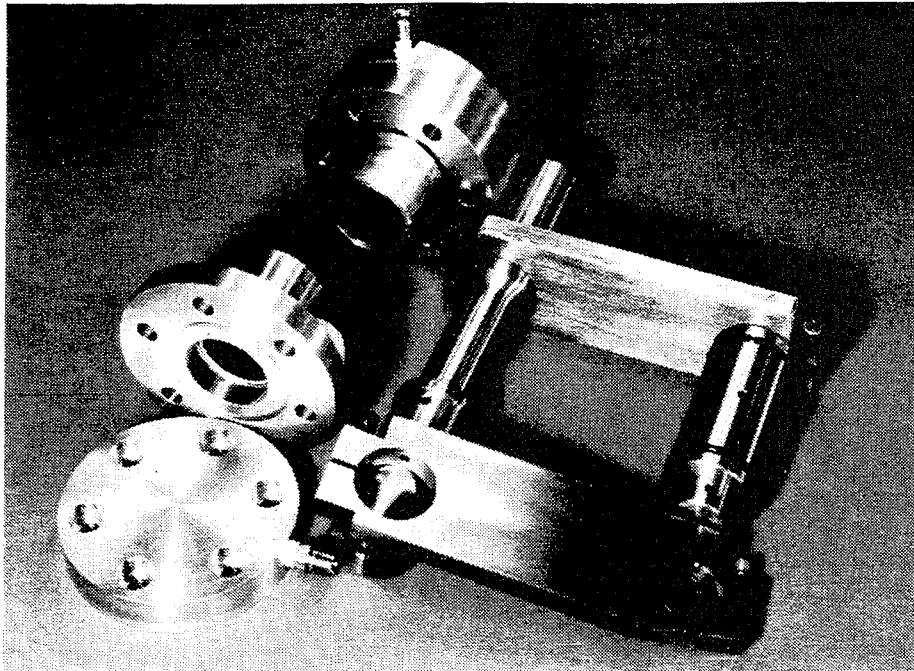


FIGURE 20. SWINGLINKS, PIVOT SHAFT AND JOURNAL BEARINGS, AND YOKE SHAFT

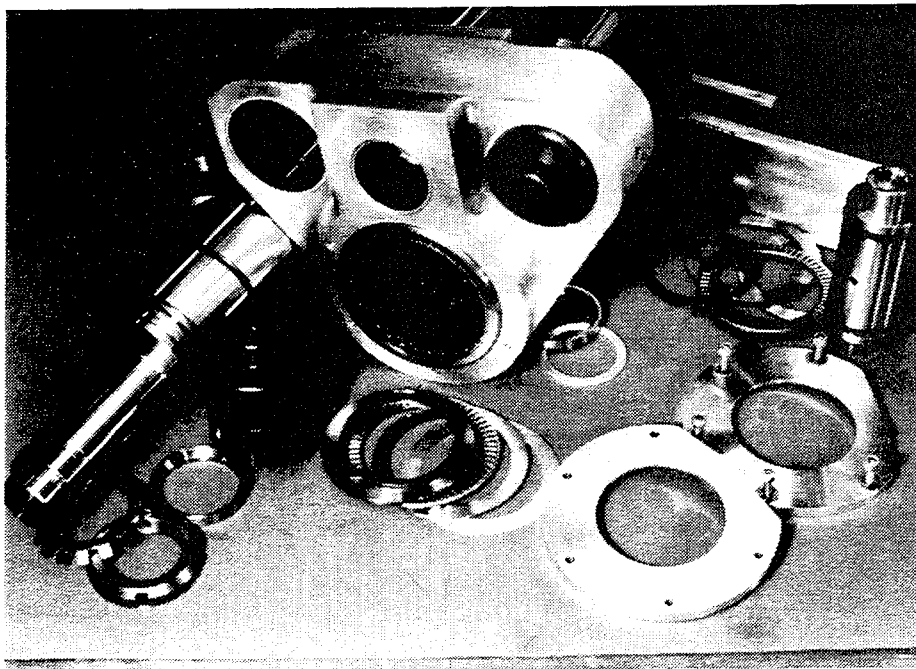


FIGURE 21. ROSS YOKE, CRANKSHAFT, BEARING, AND VARIOUS COMPONENTS

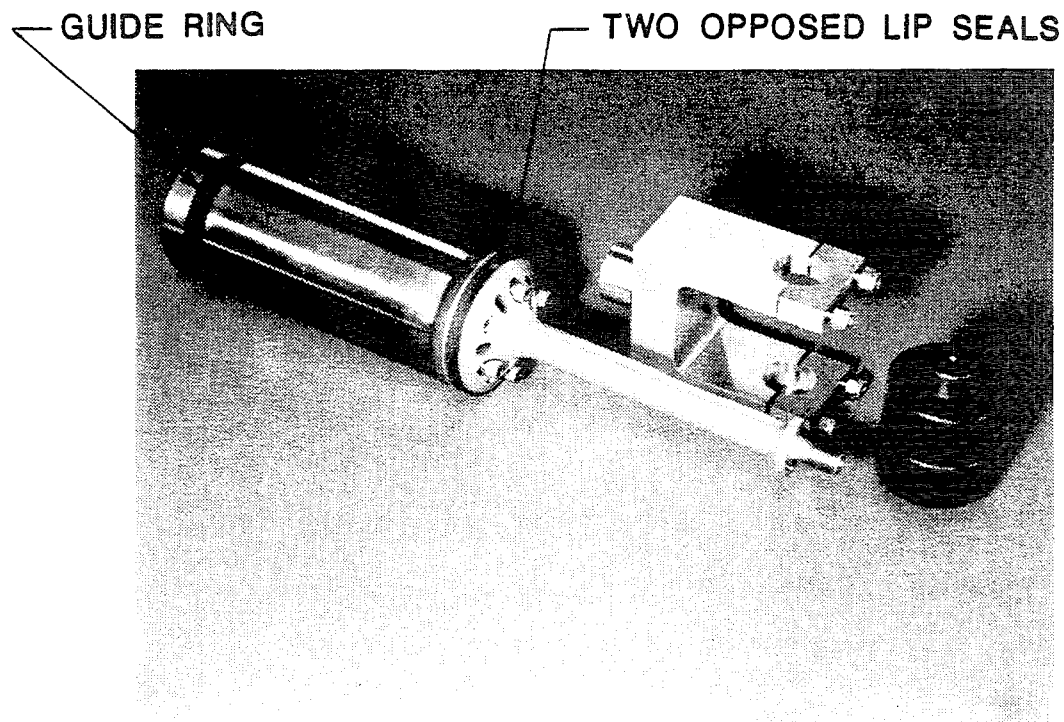


FIGURE 22. EXPANSION PISTON WITH GUIDE, LIP SEALS, TWO-PIECE CONNECTING ROD, AND JOURNAL

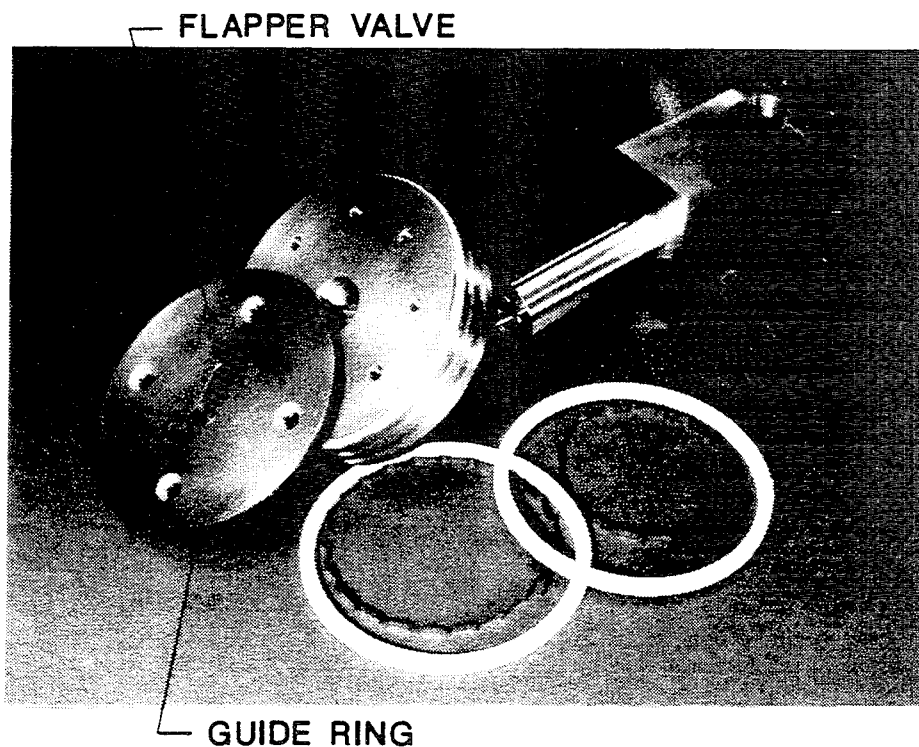


FIGURE 23. COMPRESSION PISTON, ROD, JOURNAL, AND SPLIT/SPRING LOADED SEALS

driven by the Ross yoke in a near perfect linear manner. However, because of rotation at the yoke, a bearing is employed at the rod-to-yoke connection. The journal is made from high strength 7075-T6 aluminum and is surface treated with a PTFE-impregnated hard anodize called Nituff® to provide wear resistance and compatibility with the journal bearing. The bearing, which is housed by the yoke (Figure 21), is a DU plain bearing made by Garlock Bearing Inc. These bearings consist of a steel backing, a porous bronze (filled with a lead and PTFE mixture) layer, and an overlay of lead and PTFE. The 7075-T6 aluminum connecting rod consists of two parts to allow for placement of the bellows seal.

The compression piston (Figures 14 and 23) is primarily constructed from solid high strength 6061-T6 aluminum and uses a similar bearing arrangement as the expansion piston. To the top of the piston is affixed a thin plate which holds a flapper valve and guide ring. The flapper valve allows piston blow-by gas to return to the working space. Like on the expansion piston, the guide ring is made from Rulon LD and is used to prevent metal-to-metal contact between the piston and the cylinder liner. The compression cylinder liner is 6061-T6 aluminum treated with Nituff® coating and honed to a 6 to 10 μ finish to reduce wear and friction of the seals and guide.

The compression piston carries three spring-loaded split ring seals manufactured by Tetrafluor, Inc. Initially, a nearly pure Teflon material was used for the seals but failed early during performance testing. After observing pressure fluctuations which seemed excessively high in the bellows space during testing, it was suspected that excessive piston blow-by was occurring. Disassembly for inspection revealed that the compression

piston seals were worn flush with and even recessed into the piston ring groove. Several teaspoonfuls of seal debris were found in various areas of the machine as indicated by the photographs of Figure 24. This required disassembly, cleaning, and replacement of the compression piston seals. The basic spring-loaded split seal configuration was still believed to be sound but apparently a more wear-resistant seal material is needed. New Tetrafluor seals were used which are made with a proprietary material quite similar to Rulon LD. Performance and wear of these new seals was found to be much superior to the previous seals. Also, a metal bellows seal was found to be cracked, probably as a consequence of the excessive pressure fluctuations in the bellows space due to blow-by. An existing spare metal bellows was installed to replace the one that cracked. An external buffer volume was also connected to the bellows spaces to further reduce the pressure fluctuations.

The crankcase is pressurized to the working space cycle minimum (charge) pressure of 2 MPa to offset the pressure differential and associated loads on the drive mechanism and bellows. Reducing the bearing loads reduces the mechanical losses and prolongs the life of the system. Pressure loading on the bellows is minimized because the pressure in the spaces between the pistons and bellows is the charge pressure with only minor fluctuations due to volume variation and leakage past the pistons. Pressurizing the crankcase to the cycle minimum also facilitates maintaining the system charge pressure by simply connecting the working space and the crankcase through separate check valves to a pressurized helium reservoir.

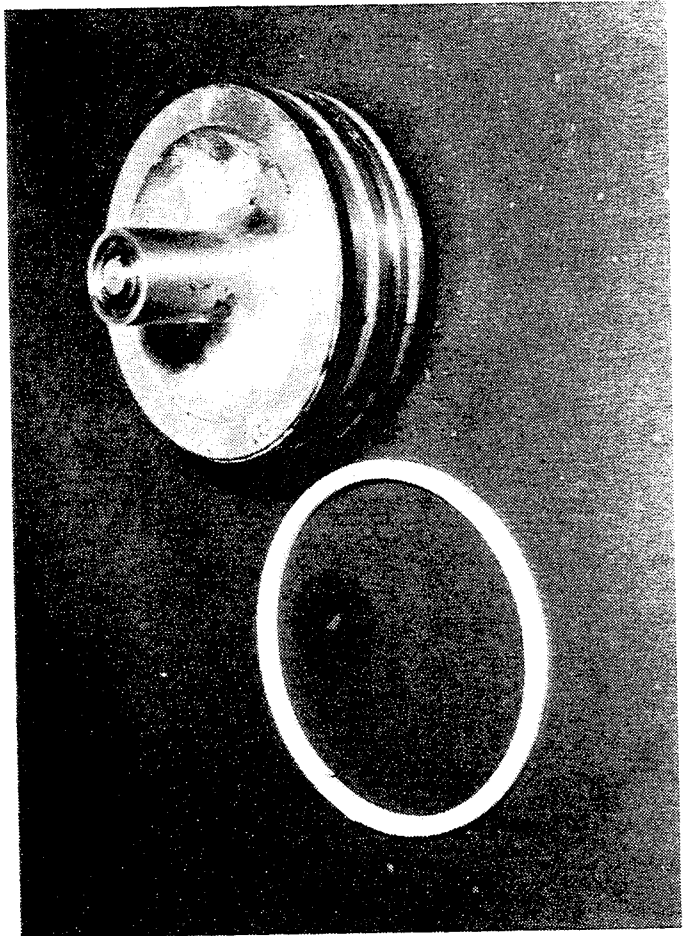
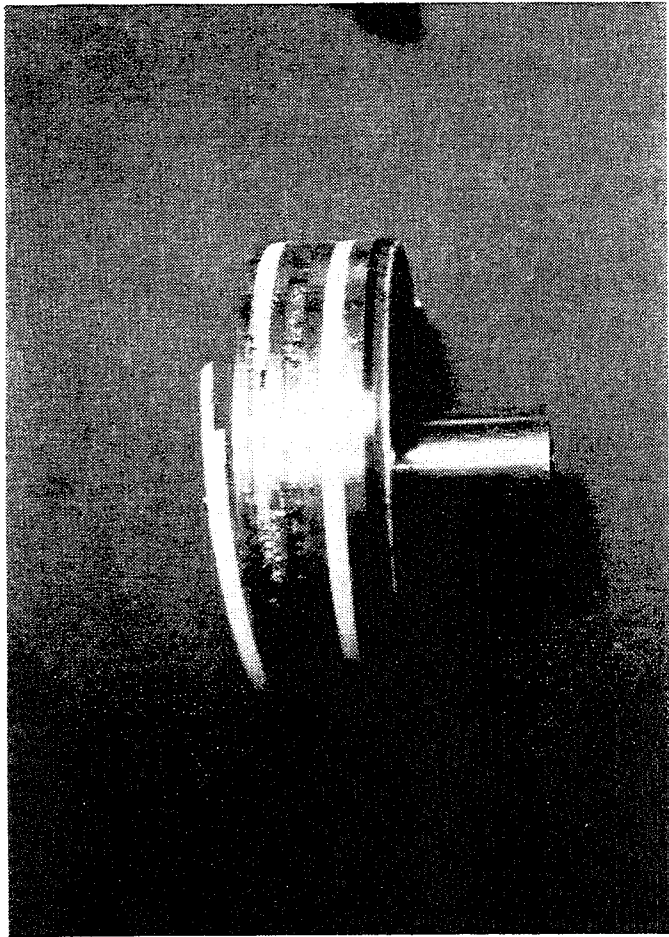
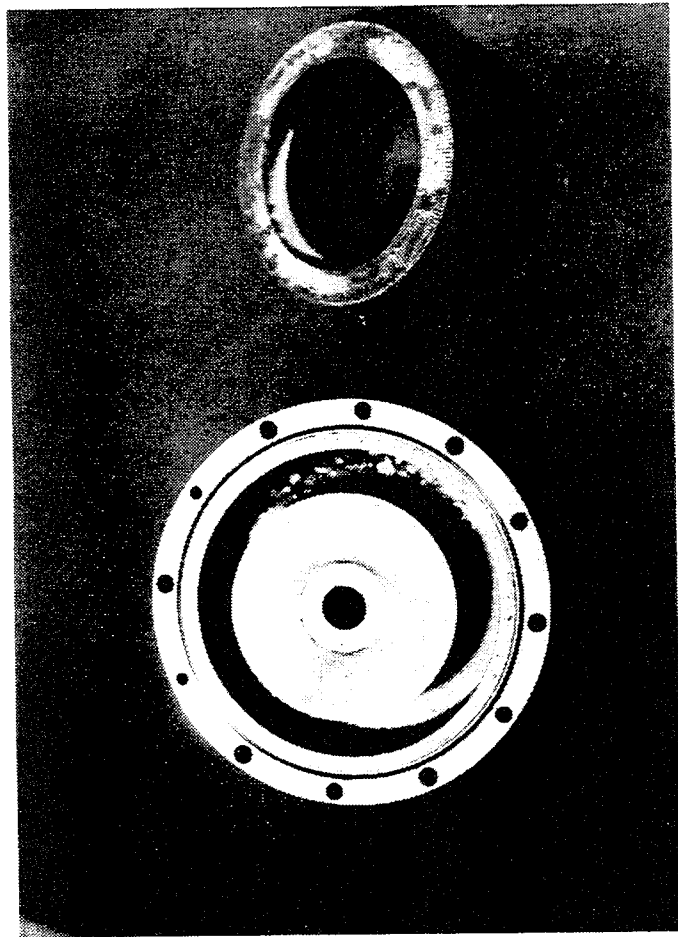


**FIGURE 24. COMPRESSION PISTON, BELLOWS,
AND REGENERATOR
CONTAMINATED BY SEAL
WEAR DEBRIS**

The feasibility prototype has a cubical crankcase fabricated from 6061-T6 aluminum plate for developmental expedience. As a consequence, relatively thick walls are required to withstand the pressurization. Further development will lead to a more efficient cylindrical crankcase.

3.4.2 Heat Exchangers

A Stirling refrigerator requires three heat exchangers:

- a) the cooler, which removes heat from the compression space;
- b) the regenerator, which acts as a thermodynamic sponge cyclically storing and releasing heat to the working fluid; and
- c) the condenser, which absorbs the heat from the refrigeration load into the expansion space.

The heat exchangers are key to a Stirling machine's power efficiency and cost effectiveness. Two critical factors are the dead volume and the thermo-fluid performance of the regenerator and cooler. Dead volume is volume in the working space, e.g. in the heat exchangers, which does not vary cyclically and therefore reduces compression ratio while promoting parasitic heat dissipation. Favorable thermo-fluid characteristics are low fluid friction and thermal conductivity in the flow (axial) direction, and high radial conductivity, surface area, and heat capacity to promote heat transfer with minimum temperature difference between the matrix and fluid.

3.4.3 Cooler

The cooler is located in the working fluid flow path between the regenerator and the compression space. It transfers the heat of compression, heat due to mechanical and

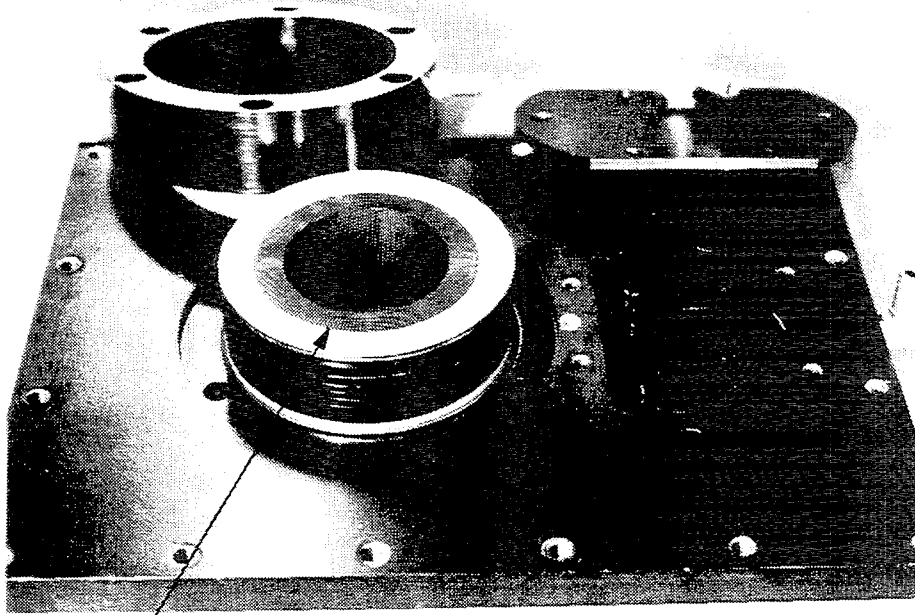
thermal parasitics, and ultimately the refrigeration heat load to the external coolant system.

As shown in Figure 1, the cooler is located near the base of the expansion cylinder and provides the gas passage between the compression space and the regenerator. An annular fin and groove configuration is used to maintain a compact system design. To remove heat from the helium working fluid, densely spaced longitudinal internal fins protrude radially inward creating vertical channels for the gas passages. Heat conducted through the aluminum fins is removed by liquid coolant. External fins protruding radially outward in a helical design create the liquid coolant flow passage. The cooler also includes liquid coolant passages in the compression cylinder head. Liquid coolant is circulated through the cooler to dissipate the heat to the ambient. The physical construction and features of the cooler are shown in Figure 25.

During testing, temperature data indicated that the metal temperature of the water jacket was higher than desired, about 60°C. It is desirable for the water jacket, which functions as the thermodynamic heat sink, to be as cool as practical. Otherwise, the refrigeration heat load has to be lifted higher, which requires more work or produces less refrigeration. To alleviate this, the coolant ports were modified to improve water circulation, and coolant passages were added in the block walls adjacent to both cylinders.

3.4.4 Regenerator

A regenerator cyclically absorbs heat from and releases heat back to the working fluid. In the ideal Stirling refrigeration cycle, the working fluid takes on heat at constant



CLOSELY SPACED INTERNAL GAS FINS

HELICAL LIQUID COOLANT FINS

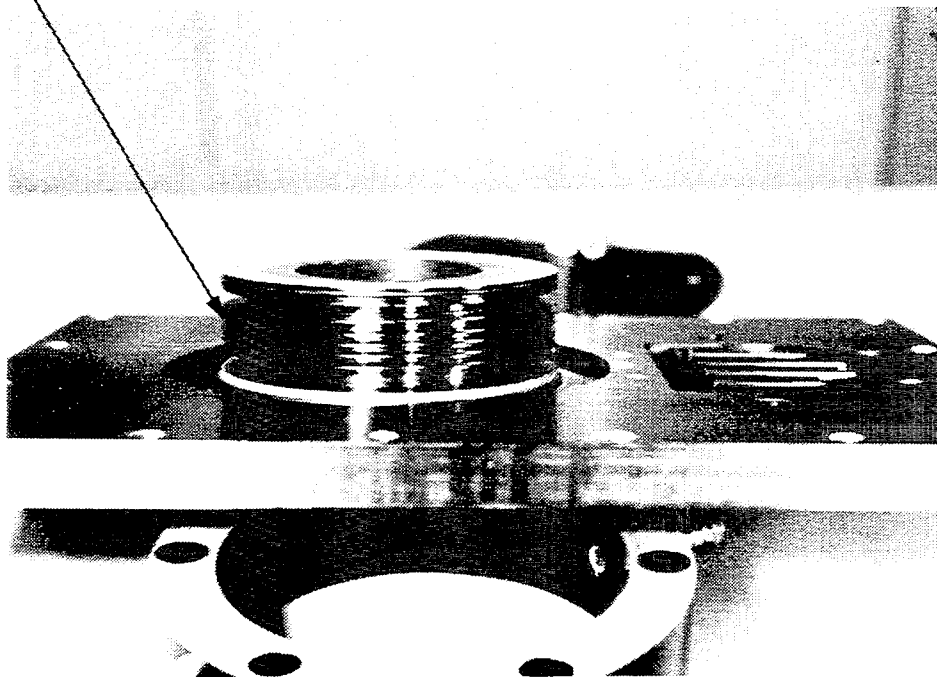


FIGURE 25. PHOTOGRAPHS OF COOLER

volume as it passes through a regenerator from a cold expansion space to a warmer compression space. Heat is rejected from the system by isothermal compression in the compression space. The working fluid then passes back through the regenerator for constant volume regenerative cooling. Heat is stored in the regenerator for transport out in the next cycle. Finally, refrigeration occurs by isothermal expansion in the expansion space where heat is absorbed by the working fluid.

In a real Stirling machine the flow surges back and forth so that little or none of the working fluid (typically helium) passes completely through the regenerator matrix. This, combined with the axial temperature gradient, complicates the energy flows so the incremental details are not well understood and theories of regenerator operation in Stirling machines are highly idealized. It is common, for example, to assume a linear axial temperature gradient and to ignore the local temperature variations in both matrix and gas that must occur. Ideally, the regenerator should have high heat capacity and heat transport capabilities such that heat exchange with the helium working fluid at a high rate does not cause significant temperature fluctuation in the regenerator. Also, the regenerator should introduce minimal axial heat conduction, flow restriction, void (compressible gas) volume, and clogging susceptibility in the helium flow path. For ideal Stirling machines, void volume increases the size required for a given power or refrigeration capacity by reducing the cycle pressure ratio but does not reduce the power efficiency or coefficient of performance. In real Stirling machines, void volume causes power losses due to heat flows resulting from compression and expansion of the gas in the void.

Regenerator ineffectiveness results from deficient heat transfer between the matrix and the working fluid due to insufficient matrix heat capacity or heat transport rate, and heat dissipation due to compression/expansion of working fluid in the regenerator void volume. Heat flow resulting from regenerator ineffectiveness directly subtracts from the refrigeration produced in a Stirling refrigerator, thereby necessitating a larger machine and greater power input for a given amount of refrigeration. The requirement for a larger machine compounds the reduction in power efficiency by proportionately increasing the void volume and heat transfer losses.

High regenerator effectiveness is critical to optimizing the power, speed, weight, size, and service life of Stirling cryocoolers. In a 100 K refrigerator with a 300 K heat sink, the regenerator is required to transfer energy at a rate of 20 watts per watt of gross refrigeration produced. Each 1 % of regenerator ineffectiveness will consume 20 % of the gross refrigeration produced. Due to the high ratio of heat cycled in a regenerator per unit of gross refrigeration produced, regenerator ineffectiveness can overwhelmingly increase required drive power and impose limits on highest operating speed and lowest refrigeration temperature.

Because of the large number of variables involved, optimal regenerator design requires testing and iterative refinement. The present regenerator in the feasibility prototype natural gas liquefier is a first-generation annular stacked wire mesh design. The regenerator and its housing are shown in Figure 26. As described in Section 3.3, REGEN3.1 computer model analyses indicate that its ineffectiveness should be only about 1%, and further refinement, if necessary, will require empirical iteration. Future alternatives to be investigated include wrapped metal foil or polymer (e.g. Vectra, Aclar, Kapton) film.

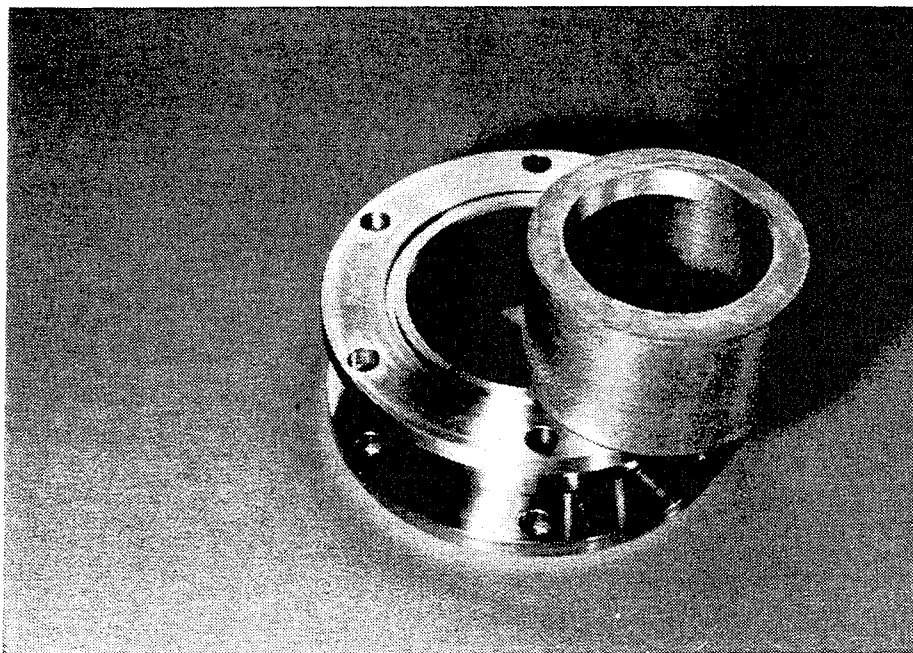
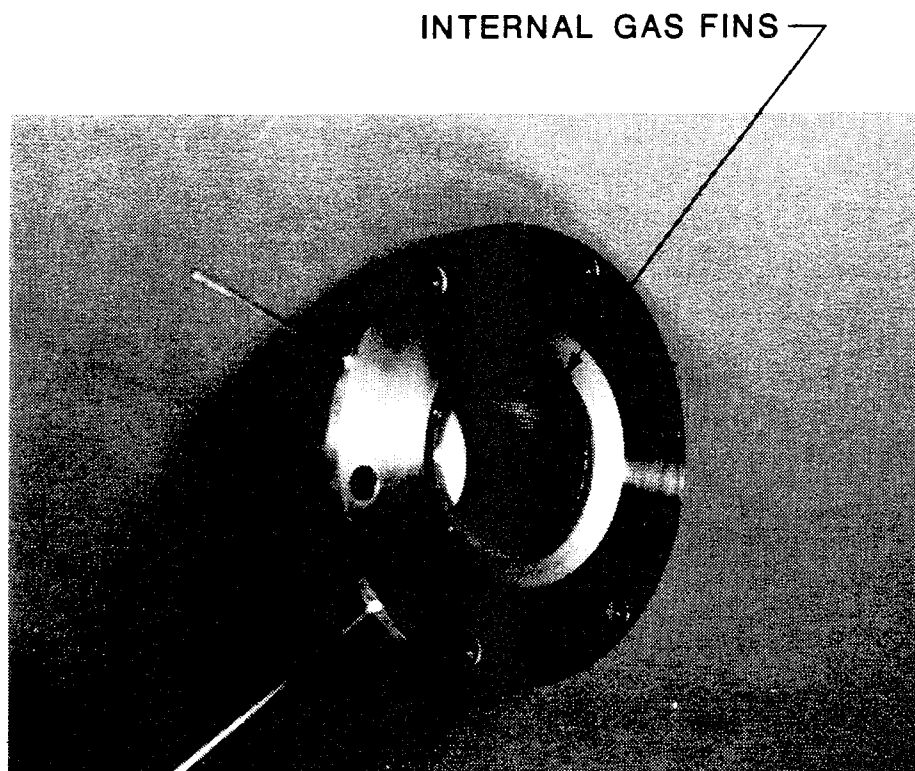


FIGURE 26. STACKED SCREEN REGENERATOR AND HOUSING



**FIGURE 27. INTERNAL VIEW OF CONDENSER DOME
(COLD HEAD)**

3.4.5 Condenser

The condenser transfers the refrigeration load (heat absorbed from the condensing natural gas) into the internal working fluid (helium) of the machine. The condenser consists of internal fins through which the helium working fluid flows between the expansion cylinder and the regenerator, and external fins exposed to the natural gas, separated by a dome-shaped pressure vessel.

The internal fins are copper radial fins that fit in the annulus between the expansion cylinder liner and the inside of the condenser dome as can be seen in Figure 1 and Figure 27. The external fins are copper radial fins which are brazed to the exterior surface of the condenser dome but are not installed on this prototype machine. The fins are sized to allow worst-case laminar film condensation of the natural gas. Fin coatings, such as teflon and various silicones, which inhibit wetting of the surfaces and promote dropwise condensation to allow additional margin for heat transfer and condensing capability, will be investigated in future development. Further development and refinement of the condenser internal and external heat exchangers will be based on test data from the existing prototype liquefier and additional thermofluid modeling.

Early in performance testing it was found that the o-ring seal between the condenser dome flange and the regenerator housing became leaky after successive cooldowns to cryogenic temperature. This was indicated by decreasing refrigeration capability as if due to increasing stray heat load. The problem was corrected by installing a metal c-ring seal between the flanges.

3.4.6 Auxiliary Equipment

Auxiliary equipment for starting, cooling and control of the natural gas liquefier system will primarily consist of commercially available automotive and natural gas service components. These components, however, are not employed at this stage of development.

The computer analyses show that approximately 6 kW of heat must be dissipated at near ambient temperature by the cooler. For system thermal efficiency, the cooler must be as compact (minimum dead volume) and as cool as practical. A liquid cooling system is more effective for this purpose than simple air cooling. An external auxiliary "radiator" is required to complete the cooling loop. The 6 kW of heat dissipation is well within the capacity of a typical automotive radiator. The radiator fan and pump will be driven by a small, auxiliary electric motor.

A solenoid valve will control gas flow to the liquefier condensing chamber. The normally-closed solenoid valve will shut off gas flow in the event of a fault condition, power loss, or turn off. Pressure buildup in the condensing chamber resulting from a fault condition will be vented by a spring-loaded relief valve.

Liquefied natural gas will drain from the condensing chamber through a flexible delivery hose like those commercially available for liquid nitrogen service. A suitable hose, available from Cryofab, Inc., consists of a double-wall, vacuum-insulated, stainless steel flexible bellows inner conduit sheathed in braided stainless steel. A 6 foot length of such hose with a 6 millimeter inner diameter has a heat loss of approximately 0.5 W.

The delivery hose will connect to the vehicle's fuel tank through a quick-connect ball coupling specially designed for LNG service. In a typical design, each half of the coupling, one on the hose and the other on the vehicle, contains a spring loaded ball valve. The coupling engages with a quarter turn of a collar that locks to prevent accidental uncoupling. The action of engagement rotates both balls to align bores through them and allow flow. The seals and seal positions are such as to prevent any leakage or spillage during and after coupling or uncoupling.

For a production natural gas liquefier system, the following features will be added to the coupling:

- o A circuit closure that allows the system to operate only when the coupling is properly engaged;
- o A tank-full (back pressure) sensor, similar to that on an automotive fuel delivery nozzle, that shuts off the system when the vehicle tank is full, or alternatively, a shutoff circuit that is activated by the vehicle's tank fuel level sensor;
- o A coupling release spring mechanism that is cocked by the action of engagement and is released by a solenoid, in response to system shutoff, to automatically disengage the coupling and allow the hose to retract from the vehicle should the driver fail to do so. The vehicle can have a safety switch at the tank coupling which prevents vehicle start-up when the hose is engaged.

3.4.7 System Operation, Control, and Safety

For residential applications, the natural gas liquefier system will be installed where the vehicle to be fueled can be parked for 6 to 8 hours, such as a carport or driveway.

Operation will be automated, requiring only that the operator connect the delivery hose to the vehicle, set a timer or select 'FILL', and press a 'START' button. The liquefier will then automatically execute a start sequence and operate until the vehicle fuel tank is full, the set time elapses, a fault condition occurs, or the operator presses a 'STOP' button.

The system will start only if the delivery hose connection is properly secured. The start signal will engage the electric motor. When operating speed is reached, a sensor will monitor for the condensing chamber temperature to reach 100 K which will signal for the solenoid valve to admit natural gas to the condensing chamber. The gas entering the condensing chamber will condense to liquid and drain into the delivery hose, cooling it and evaporating back into the condensing chamber until the delivery hose is cool enough to pass liquefied gas into the vehicle fuel tank. A one way check valve downstream of the gas admission solenoid valve will prevent any backflow from the condensing chamber to the gas main in the event of a sudden pressure surge or blockage of the delivery hose.

The crankcase pressure and cooling water temperature will also be monitored. If the delivery hose connection is interrupted, if shaft speed, condensing chamber temperature, crankcase pressure, or cooling water temperature do not remain within proper limits, or if the selected time elapses or the vehicle tank fills, the natural gas admission valve will close, drive motor power will be shut off, the delivery hose will disengage and retract from the vehicle, and a corresponding control panel status light will indicate the condition. Over-pressurization of the system will also be prevented by check valves which vent the refrigerator working space (helium) into the crankcase, and pressure relief valves which will limit crankcase pressure.

4.0 TEST INSTRUMENTATION AND PROCEDURES

Testing of the prototype NGL began with low pressure leak testing of the bellows, the crankcase/block, and the refrigerator cylinder head subassembly. The crankcase/block and the cylinder head were separately subjected to high pressure (hydrostatic) integrity testing. In operation, the cylinder head is subjected to higher pressure (charge plus cycle pressure) than the block (charge pressure only).

After the foregoing static pressure tests were successfully completed, the drive mechanism and pistons were installed in the crankcase/block for alignments and mechanical operation checkouts. The crankshaft was then driven to increasing speeds to verify proper mechanical operation. With the cylinder liners in the block to guide the pistons, and the cylinder head removed to preclude compression, seal friction and drive mechanism losses were measured.

Following mechanical checkouts and after meticulous cleaning, the assembly was completed and a series of prolonged evacuations and purges carried out. This procedure was first performed with nitrogen and then helium to flush air and moisture from the system prior to charging with helium.

Photographs of the prototype NGL performance test setup and instrumentation are shown in Figure 28. The NGL was driven by an external 10 HP AC drive motor as shown in Figure 29. A production version of the NGL would have a direct drive motor which would be hermetically integrated with the crankcase. For the prototype, however, it was expedient to use a dual V-belt/sheave drive approach and a large flywheel as shown in Figure 30. An oversized flywheel was used because it was on hand, precluded the need

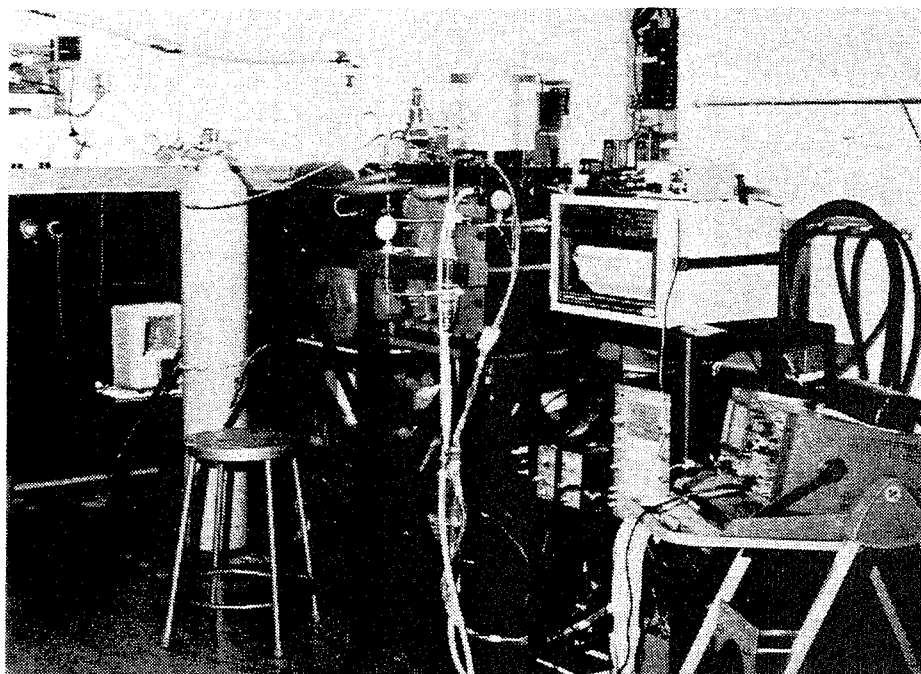


FIGURE 28. PROTOTYPE NGL TEST SETUP

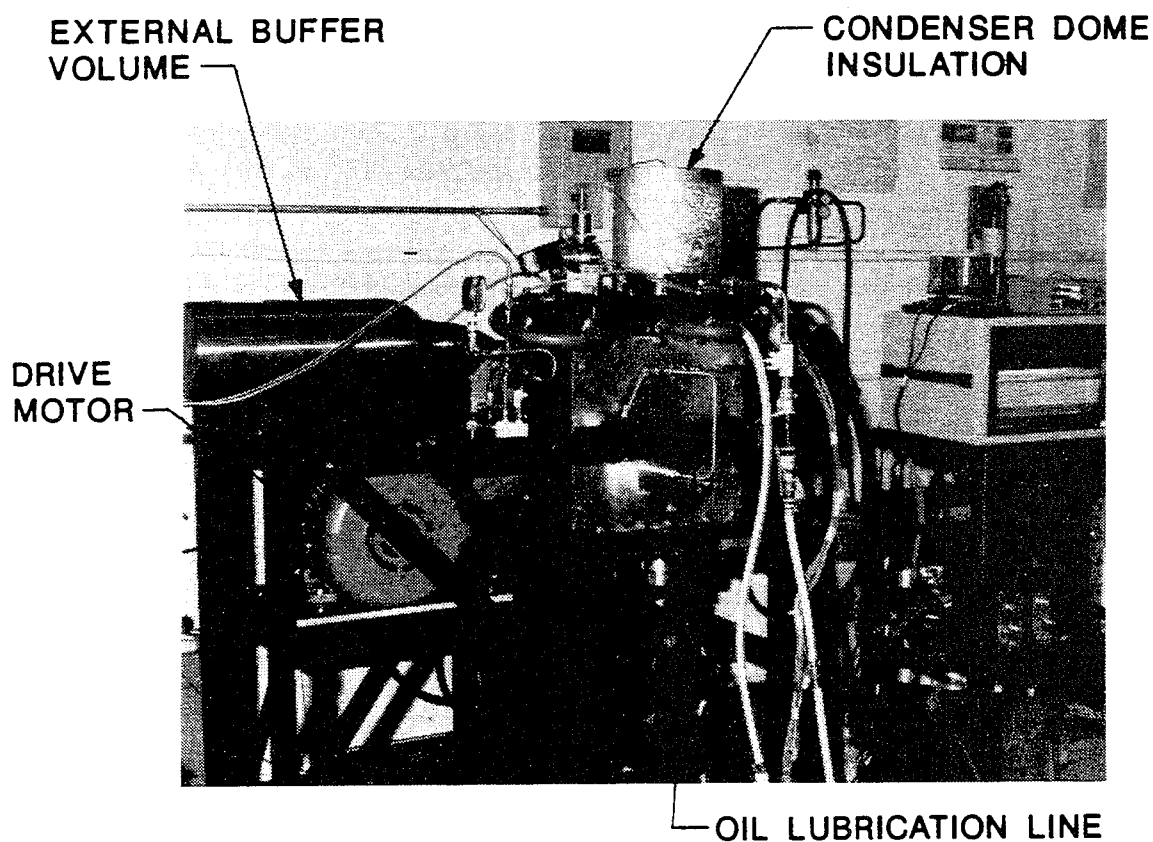


FIGURE 29. VARIOUS FEATURES OF TEST SETUP

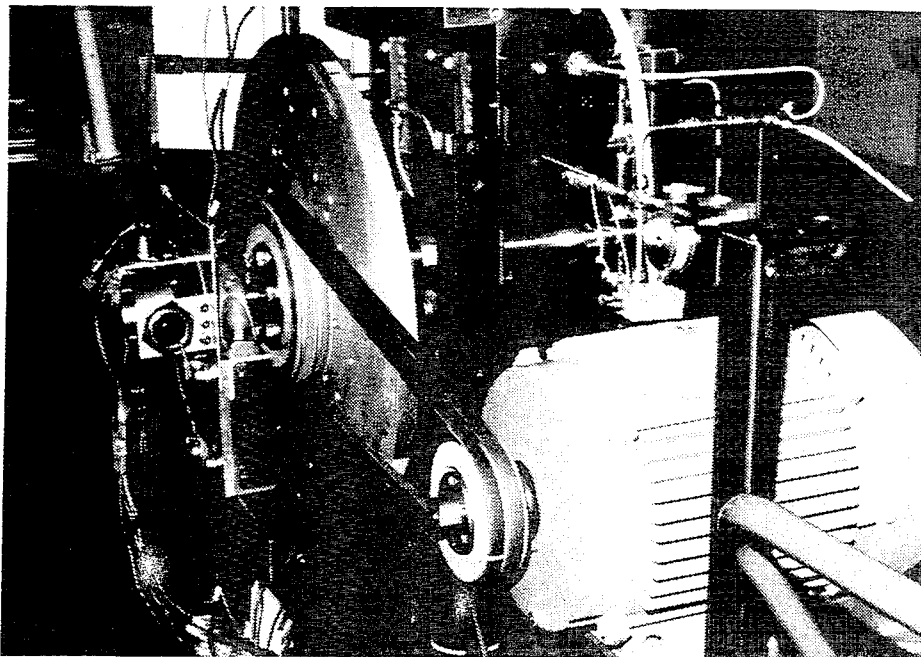
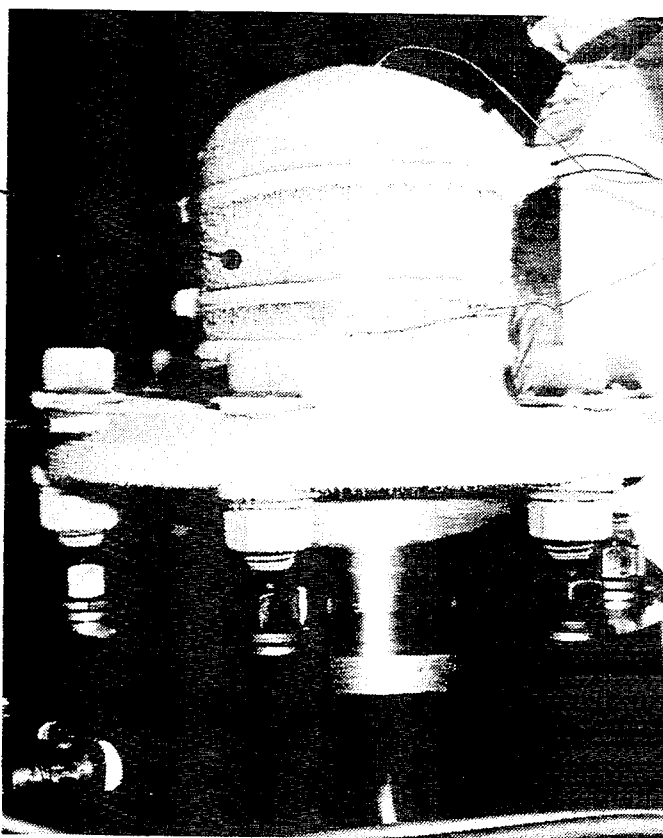


FIGURE 30. V-BELT DRIVE ARRANGEMENT FOR NGL

HEATING
ELEMENT



**FIGURE 31. HEATER WRAPED AROUND CONDENSER DOME
WITH FROST DUE TO REMOVAL OF
INSULATION AFTER TEST**

for inertia sizing analysis, and allowed convenient placement of reference marks. Motor input power was calculated from phase current and voltage measurements and power factor data.

Open loop tap water flow was used to remove heat from the cooler. Water flow rate and inlet and outlet temperatures were measured. This data allowed calculation of the power dissipation from the cooler, which should equal the shaft power input plus the total external heat refrigeration load less any heat dissipated to the ambient by free convection. Knowledge of the motor shaft power (from motor input power measurements and efficiency curves) and the applied heat refrigeration load allowed approximate calculation of the stray external heat load for comparison with previous measurements of non-operating stray external heat load on the cold dome.

The rate at which natural gas can be liquefied is directly proportional to how much refrigeration heat load the condenser dome can absorb at liquid natural gas temperature. In lieu of condensing natural gas, the refrigeration load was determined by measuring how much electrical power could be dissipated from a heating element while monitoring the condenser temperature. The heater strip was wrapped around the circumference of the condenser dome as shown in Figure 31. During operation the heat was conducted radially inward as would normally occur with external condensing fins. The condenser dome temperature was monitored by thermocouples installed on the top and side of the dome under the heater strip.

Thermocouples were also placed to measure gas temperatures in the passages at the warm and cold ends of the regenerator and at the compression space, and to

measure crankcase and oil temperatures. All temperatures were plotted on a data logger chart recorder. In addition, stick-on temperature indicating patches were placed on the Ross yoke, expansion piston rod, and crankshaft support bearing housing for later disassembly inspection.

A dynamic pressure transducer was connected to the compression space to monitor the basic pressure cycle and provide an analog signal for thermodynamic analysis. A dynamic differential pressure transducer was connected between the expansion and compression spaces (as shown in Figure 32) to measure pressure losses across the regenerator and cooler in real time. Bellows space pressure, crankcase pressure, and oil pressure were monitored by bourdon dial gauges. Charge pressure was controlled from a regulated tank of compressed helium connected to the bellows space and through a check valve to the crankcase.

A novel approach was used to generate P-V diagrams in real time for diagnostic and thermodynamic performance analysis. A cam on the crankshaft and two proximity sensors (as shown in Figure 33) plus appropriate conditioning electronics were used to generate dynamic analog signals of the expansion, compression, and/or total volume cycles. These signals were combined with the dynamic pressure sensor signal to generate P-V diagrams in real time. The expansion space P-V diagram represents the gross refrigeration produced by the cycle. The compression space P-V diagram shows the compression work required, which includes work returned to the cycle by the expansion process in absorbing the refrigeration heat load. The total-volume P-V diagram indicates the net input work absorbed by the cycle. Correlation of the expansion space

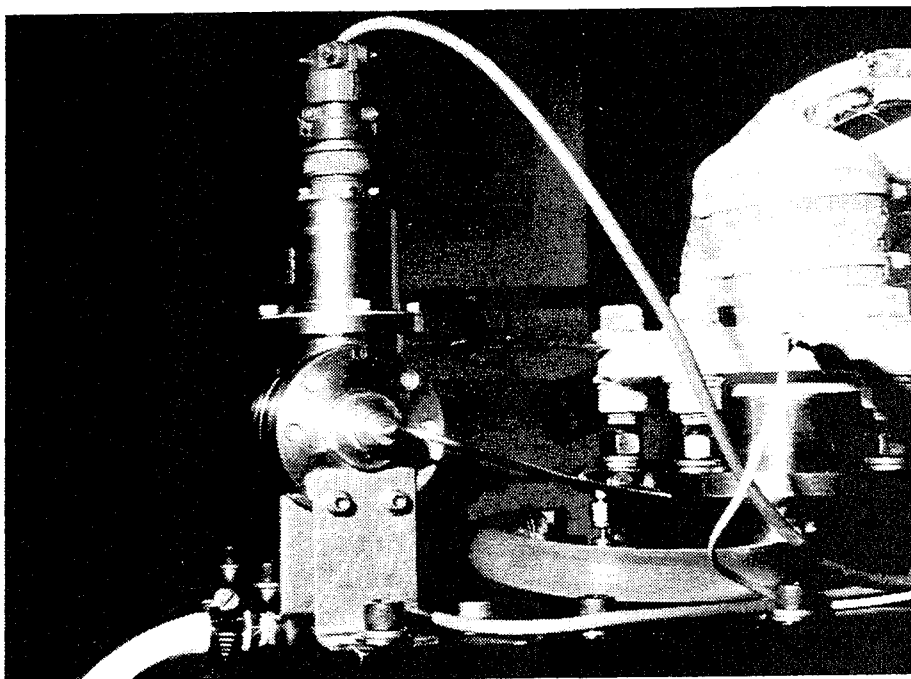


FIGURE 32. DIFFERENTIAL PRESSURE SENSOR INSTALLED ON PROTOTYPE NGL

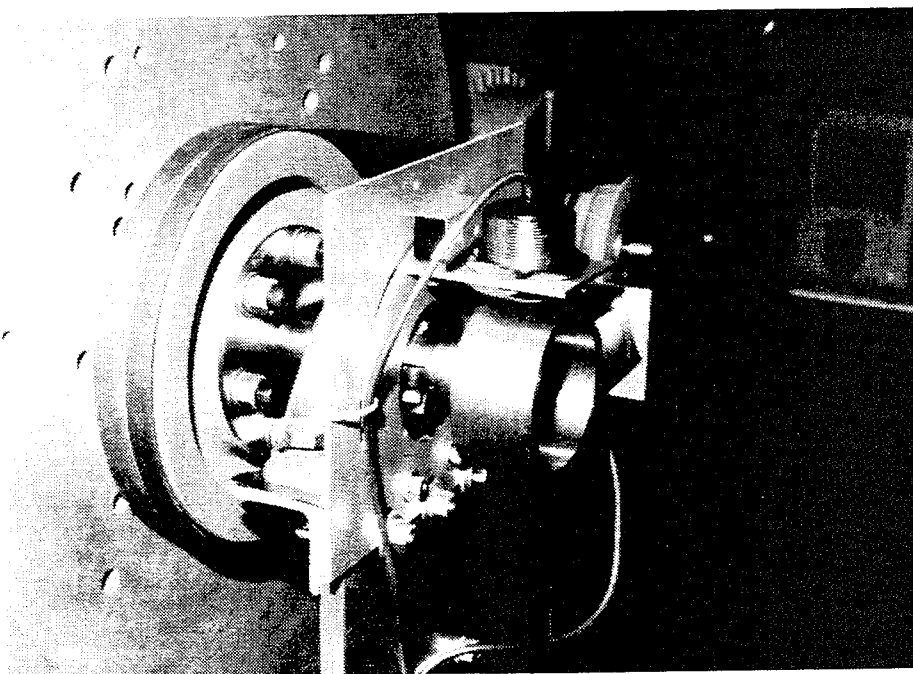


FIGURE 33. PROXIMITY SENSORS/CAM ARRANGEMENT USED TO GENERATE ELECTRICAL ANALOG OF WORKING VOLUMES

P-V diagram with the applied and stray external heat loads indicates the magnitude of internal parasitic heat loads such as from regenerator ineffectiveness and internal conduction and convection. Comparison of the total-volume P-V diagram with motor power and performance data (to derive shaft power delivered) shows power lost to internal mechanical and fluid flow friction.

Refrigerator performance tests were conducted at systematically varied combinations of charge pressure, operating speed, and refrigeration load. During performance testing, the refrigerator working space, bellows space, and crankcase pressures were monitored. Once each cooldown was achieved, net refrigeration capacity was measured by increasing the power to the electric heater applied to the refrigerator cold dome until the dome temperature would no longer return to below 110 K. Dynamic pressure cycle and shaft angle signals were combined to generate pressure-volume diagrams which represent the gross refrigeration produced and thermodynamic work absorbed. Measurement of cooling water flow and temperature rise showed the total power dissipation. These measurements combined with those of applied heat load and drive motor power allowed evaluation of thermodynamic and mechanical losses and system performance.

Previous tests were conducted to determine the non-operating ambient parasitic heat loads. This was accomplished by submerging the refrigerator cold dome in an insulated container of liquid nitrogen and measuring the boil-off rate as indicated by the sequential temperature rises of the thermocouples positioned along the cold dome. Liquid nitrogen boil-off rates were also measured from the insulated container alone and

from a container placed in the insulated housing which enclosed the refrigerator cold dome during performance tests. Each test was repeated to confirm that steady-state conditions were established.

5.0 TEST RESULTS

Extensive performance testing was conducted to characterize the NGL refrigeration capability and to collect data for diagnostic purposes. An objective of performance testing was to map the prototype NGL performance over a range of speed and charge pressure combinations for correlation with analyses and computer simulations. The results were to determine the best combination of speed and charge pressure, as well as to identify deficiencies and means for refinements.

Results of refrigeration capability tests conducted at various speeds and pressures plotted in a load line manner are shown in Figure 34. The data show the expected trend that for higher speeds and charge pressures more refrigeration is produced. Thus, by extrapolating from the 2 data points for operating at a charge pressure of 300 psig and speed of 1000 rpm, it appears that the highest net refrigeration capacity at the liquid methane (LCH_4) temperature of 112 K would be about 550 watts. However, it was not possible to operate the machine specifically at 300 psig and 1000 rpm with a (lower) refrigeration load of 550 watts because the greater drive power required (due to less power derived from the heat absorbed) exceeded the drive motor capacity. The coldest refrigeration temperature reached was 76 K at a charge pressure of 180 psig. However,

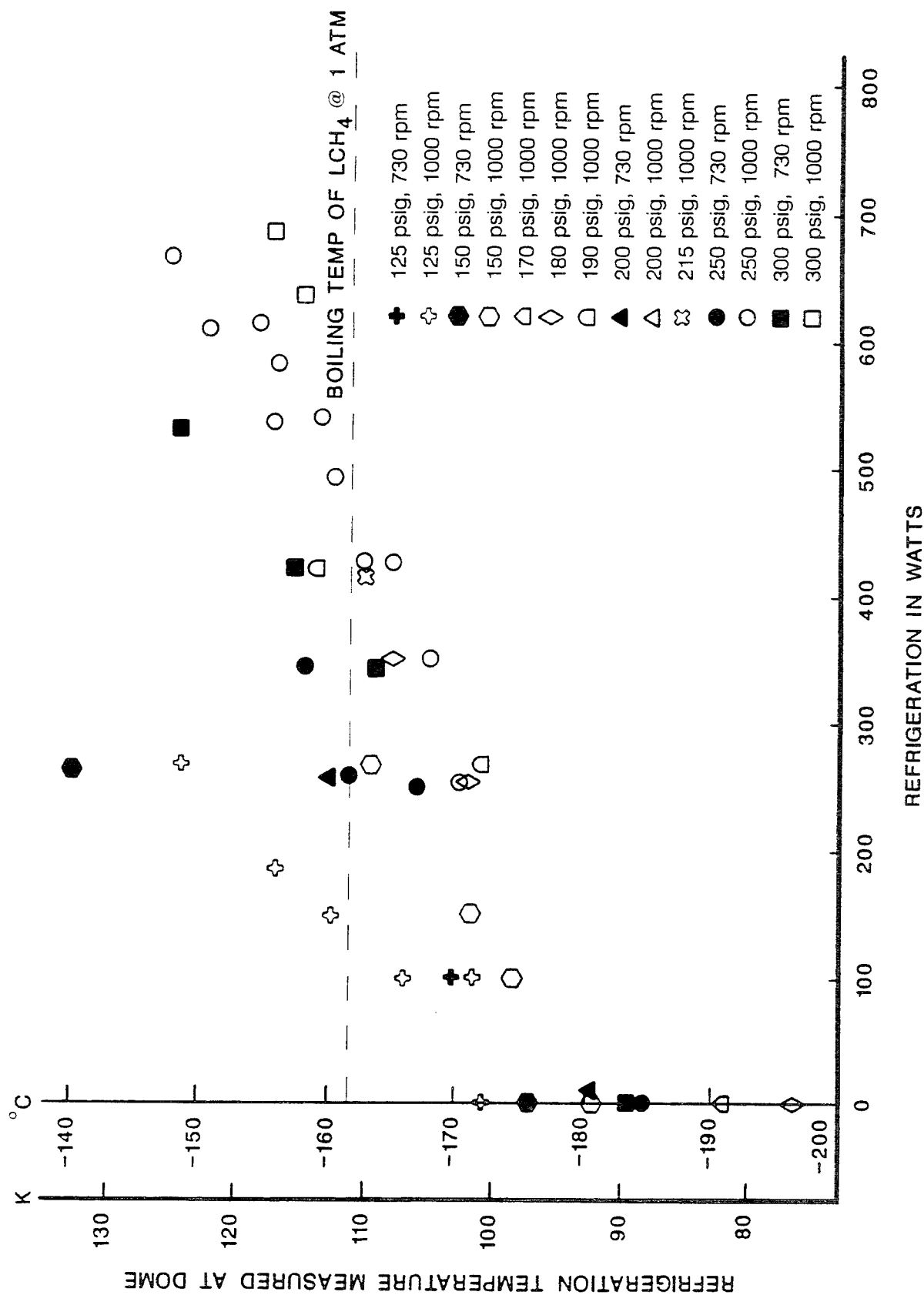


FIGURE 34. LOAD LINE PLOT OF REFRIGERATION TEMPERATURE vs APPLIED REFRIGERATION HEAT LOAD

no special emphasis was placed or extra care taken to achieve temperatures much lower than the LCH_4 temperature. The net refrigeration capacity of 550 W is much greater than achieved during testing prior to this program but still below the goal of approximately 1 kW. Much of the discrepancy is probably due to stray internal and external heat loads.

A standard indicator of efficiency is the ratio of refrigeration to input power which is referred to as the coefficient of performance (COP). The theoretic maximum (Carnot) COP is equal to the absolute refrigeration temperature divided by the difference between the heat sink and refrigeration temperatures. For refrigeration at 112 K with a heat sink at 300 K, the Carnot COP would be 0.6. In real machines the COP is also temperature dependent but is much smaller for a given set of temperature conditions than the Carnot COP. To take into account the variation in refrigeration temperature occurring during various tests (as shown in Figure 34) the actual COP was normalized by the Carnot COP for each refrigeration temperature. The net normalized COP, based on applied heat load and input power, is plotted as a function of charge pressure in Figure 35. Because parasitic heat loads are not taken into account and do not increase proportionately with refrigeration capacity, the normalized COP at low pressures appears much lower than at higher pressures. The best normalized COP attained was about 0.16, compared to a goal of about 0.4. Therefore, further significant improvement is needed for power efficient operation.

From the test data it is apparent that both the refrigeration capacity reached and the COP achieved fall short of goals and investigation is necessary. Cycle pressure ratio was examined for several test cases and appears normal or slightly better (1.87) than

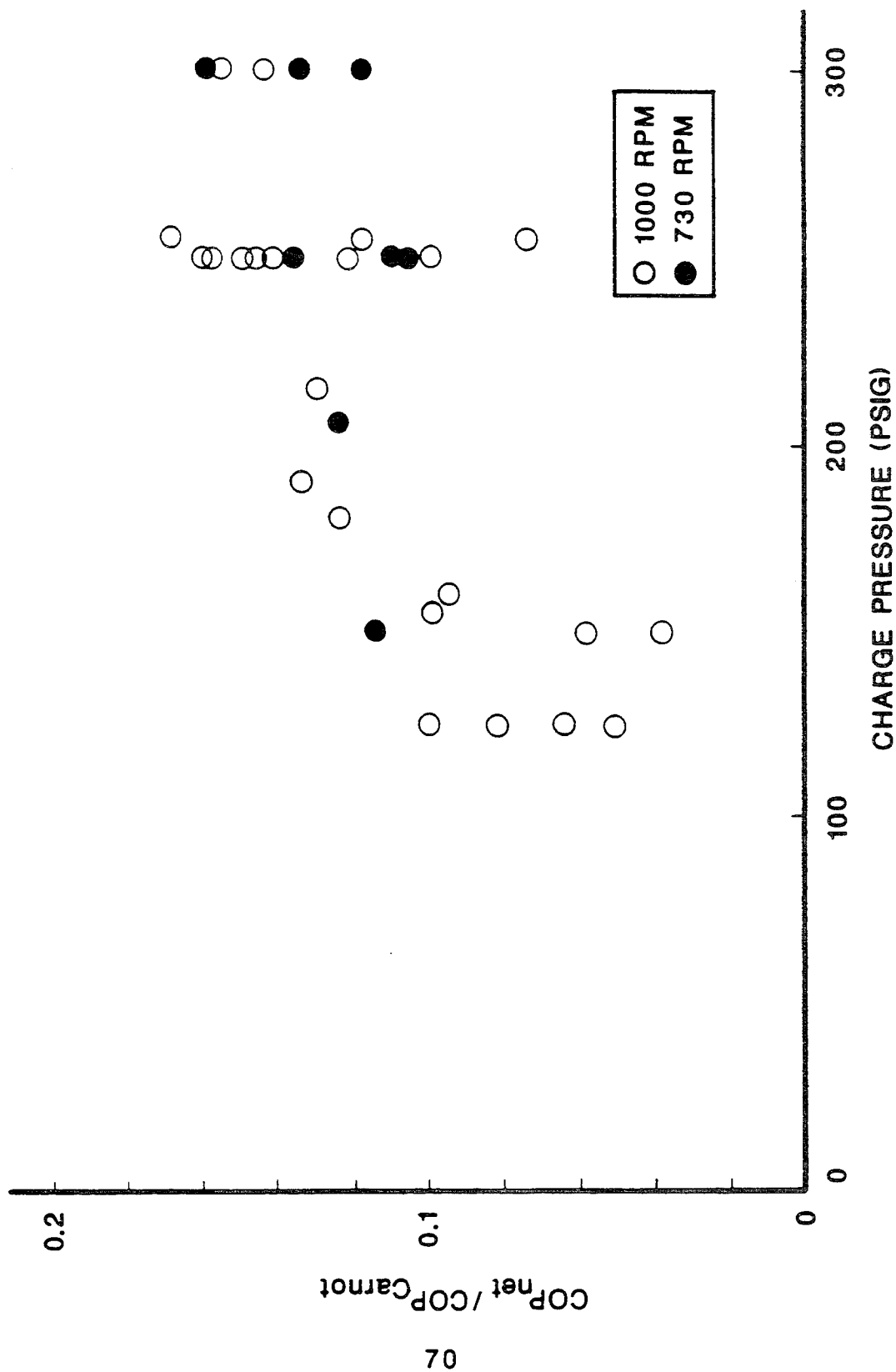


FIGURE 35. NORMALIZED COP vs CHARGE PRESSURE

predicted by computer simulation (1.83). A typical pressure cycle is shown in Figure 36 for a charge pressure of 300 psig (2 MPa).

As discussed in the previous section and shown in Figure 33, instrumentation made it possible to record actual P-V diagrams during operation. Tracings of P-V diagrams for a representative test run at a charge pressure of 250 psig are shown in Figure 37. The area enclosed by the expansion-volume P-V trace multiplied by an appropriate scale factor equates to a gross refrigeration of 1549 W. The area enclosed by the total-volume P-V trace is equivalent to a thermodynamic power input of 5054 W. The COP based on these diagrams is about 0.31. For this particular test point a heat load of 345 W was applied and 6377 W of shaft input power was required, resulting in a net actual COP of 0.054. Several adjustments must be made for purposes of comparison to the P-V indicated COP which is based on gross refrigeration and thermodynamic input power (not including drive mechanism losses). For example it is estimated from previous tests that the parasitic heat load was about 200 W and mechanical friction was 477 W. This results in a COP of $(345 + 200)/(6377 - 477) = 0.09$. However, for this particular test point 1549 W of refrigeration are indicated by the P-V diagram but only about 545 W are accounted for. This discrepancy of about 1000 W must be due to stray heat loads and internal thermodynamic losses. One probably dominant factor is that actual regenerator effectiveness is somewhat smaller than predicted by the REGEN 3.1 computer simulations. It is estimated that, for the 112 K refrigeration temperature and 300 K heat sink temperature, each percent of regenerator ineffectiveness causes a 20 percent loss in refrigeration. Regenerator ineffectiveness causes an enthalpy flow from the warm to the cold end of the regenerator, effectively placing a heat load on the system.

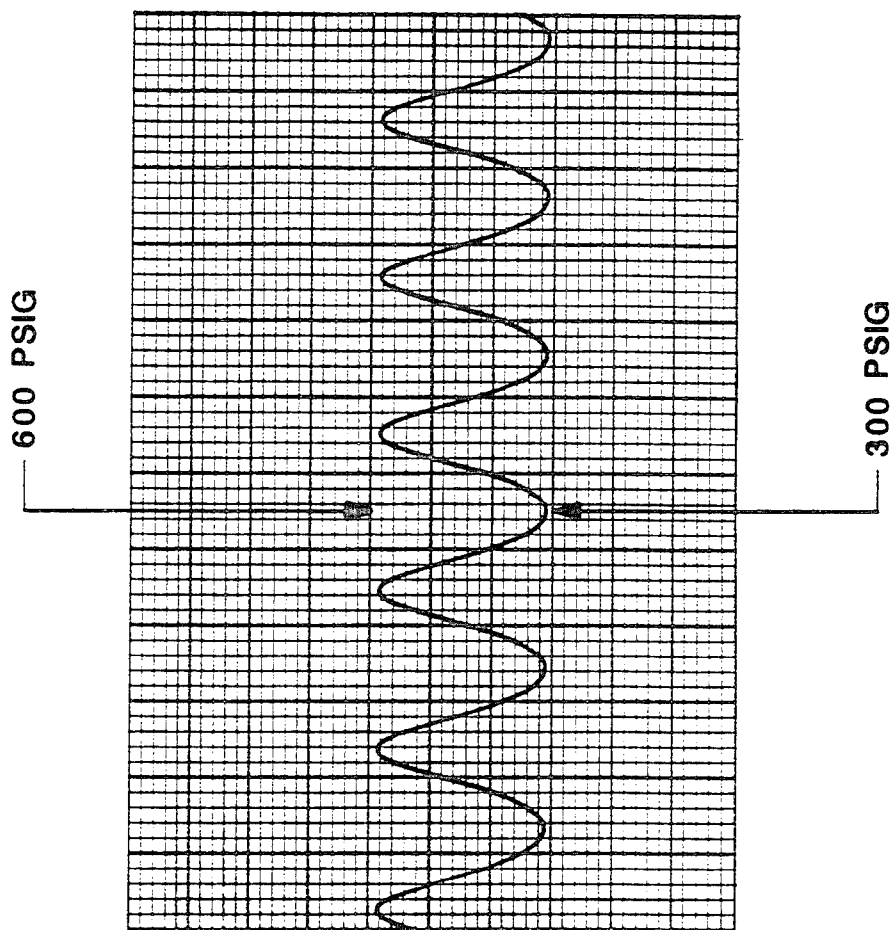


FIGURE 36. TYPICAL CYCLE PRESSURE STRIP CHART

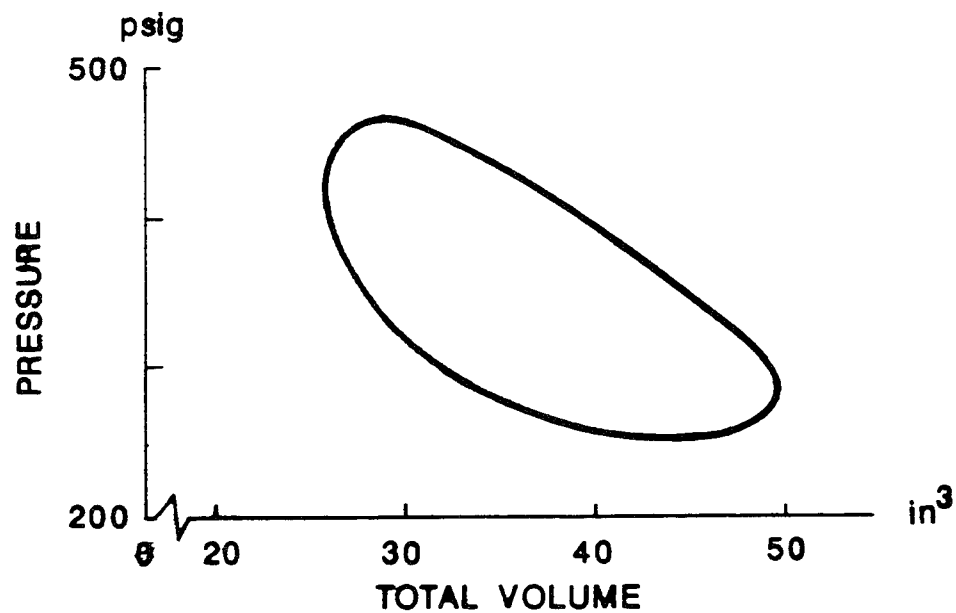
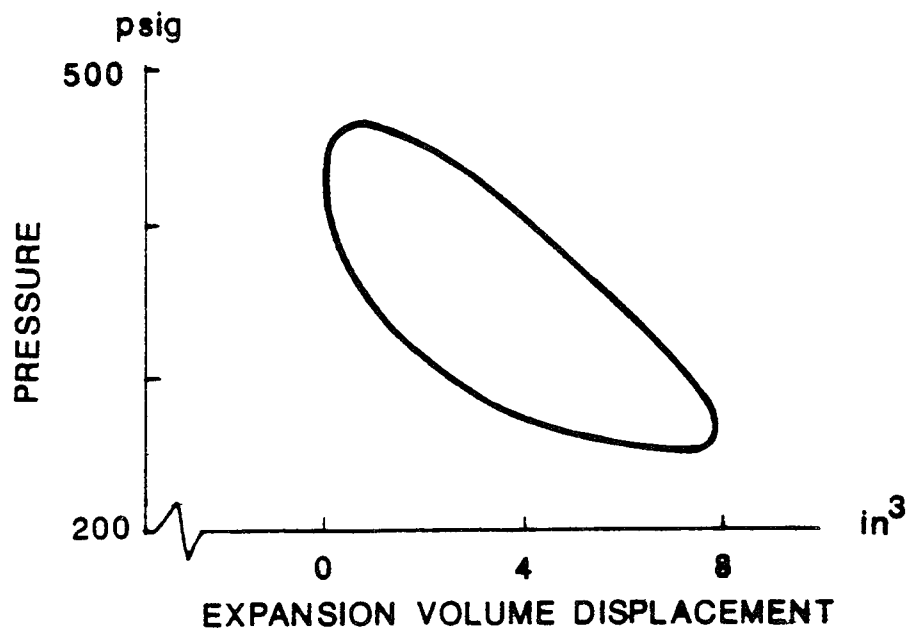


FIGURE 37. PRESSURE-VOLUME DIAGRAMS FROM DATA

Since the 1000 W unaccounted for is a 65 % loss in refrigeration, the corresponding regenerator ineffectiveness would be 3.2 %.

At the time of this report writing, a disassembly inspection of the prototype NGL had not been completed following conclusion of performance testing. Bearing wear, seal wear, and other aspects of the drive mechanism and machine will be inspected during future disassembly. However, at the conclusion of testing the machine was running smoothly and there was no reason to suspect that the mechanism did not hold up quite well.

6.0 CONCLUSIONS AND RECOMMENDATIONS

This program has substantially furthered the development of the General Pneumatics small-scale NGL and Stirling refrigerators in general. Testing was completed with only minor difficulties, and refrigeration performance was significantly improved over what was attained prior to this program but was still not at a level high enough to meet objectives.

Although this program was moderately successful, further development is needed to improve performance to achieve cost effective operation. Extended testing is necessary to assess the reliability of the fundamental components such as bearings and seals. Further analysis is needed to correlate test data with REGEN3.1 analyses to achieve a better optimized regenerator design for a second generation prototype. When these fundamental issues are resolved development can concentrate on complete system integration and production versions of the NGL.

DISTRIBUTION LIST

Department of Defense

| | | | |
|---|----|---|---|
| DEFENSE TECH INFO CTR CAMERON STATION ALEXANDRIA VA 22314 | 12 | ODUSD ATTN: (ES) CI 400 ARMY NAVY DR STE 206 ARLINGTON VA 22202 | 1 |
| ODUSD ATTN: (L) MRM PETROLEUM STAFF ANALYST PENTAGON WASHINGTON DC 20301-8000 | 1 | DIR ADV RSCH PROJ AGENCY ATTN: ARPA/ASTO 3701 N FAIRFAX DR ARLINGTON VA 22203-1714 | 1 |

Department of the Army

| | | | |
|---|------------------|---|--------|
| HQDA ATTN: DALO TSE PENTAGON WASHINGTON DC 20310-0103 | 1 | CECOM RDEC C2SID SOUTH ATTN: AMSEL RD C2 PP P AMSEL RD C2 PP PA 10108 GRIDLEY RD STE 1 FT BELVOIR VA 22060-5815 | 1 1 |
| CDR AMC ATTN: AMCRD S 5001 EISENHOWER AVE ALEXANDRIA VA 22333-0001 | 1 | DIR ARMY RSCH LAB ATTN: AMSRL CP PW 2800 POWDER MILL RD ADELPHIA MD 20783-1145 | 1 |
| CDR ARMY TACOM ATTN: AMSTA TR NAC AMSTA TR R AMSTA TR M AMSTA TR M (R MUNT) WARREN MI 48397-5000 | 1 1 1 1 | CDR ARO ATTN: AMXRO EN (D MANN) RSCH TRIANGLE PK NC 27709-2211 | 1 |
| DEPARTMENT OF THE ARMY MOBILITY TECH CTR BELVOIR ATTN: AMSTA RBF (M E LEPERA) AMSTA RBXA (R E TOBEY) 10115 GRIDLEY RD STE 128 FT BELVOIR VA 22060-5843 | 10 1 | PROG MGM MOBILE ELEC PWR ATTN: AMCPM MEP 7798 CISSNA RD STE 200 SPRINGFIELD VA 22150-3199 | 1 |

Department of the Navy

| | | | |
|---|---|---|---|
| DIR LOGISTICS PLANS & POLICY/ STRATEGIC SEALIFT PROG DIV (N42) ATTN: N420 2000 NAVY PENTAGON WASHINGTON DC 20350-2000 | 1 | CDR NAVAL RSCH LABORATORY ATTN: CODE 6181 WASHINGTON DC 20375-5342 | 1 |
| CDR NAVAL SURFACE WARFARE CTR ATTN: CODE 859 3A LEGGETT CIRCLE ANNAPOLIS MD 21402-5067 | 1 | | |

Department of the Air Force

AIR FORCE WRIGHT LAB
ATTN: WL/POSF
1790 LOOP RD N
WRIGHT PATTERSON AFB
OH 45433-7103

1

SA ALC/SFT
1014 BILLY MITCHELL BLVD STE 1
KELLY AFB TX 78241-5603

1

Other Federal Agencies

NASA
LEWIS RESEARCH CENTER
CLEVELAND OH 44135

1

DOE
CE 151 (MR RUSSELL)
1000 INDEPENDENCE AVE SW
WASHINGTON DC 20585

1

NIPER
PO BOX 2128
BARTLESVILLE OK 74005

1